7 September 2026

A Generalized Theory for the Structural and Spatial Mapping of Energy, Entropy, and Free Energy

Michael K. Gilson[1], Joe Cruz[2], Kunhuan Liu[1], Samrat Lohar[2], Helmut Carter[3], Daniel Roe[4], Tom Kurtzman[5,6]

1. Skaggs School of Pharmacy and Pharmaceutical Sciences, University of California San Diego
2. Ph.D. Program in Chemistry, The Graduate Center of the City University of New York
3. Ph.D. Program in Biology, The Graduate Center of the City University of New York
4. Laboratory of Computational Biology, National Heart, Lung, and Blood Institute, NIH
5. Ph.D. Programs in Biochemistry, Biology, and Chemistry, The Graduate Center of the City University of New York
6. Department of Chemistry, Lehman College, The City University of New York

Abstract

Systems in which the free energy density is nonuniform in space are familiar; the surface tension of a water droplet and the surface energy of a solid are good examples. Some such cases can be treated with prior theory, notably inhomogeneous solvation theory (IST), but IST is applicable only to liquids. Despite this limitation, IST has proven useful as a guide to the design of ligands to bind a targeted protein, based on the idea that ligands which displace high free energy water will tend to bind more tightly, other things being equal. Here, we present Generalized Thermodynamic Mapping (GTM) theory, a more general theory that is applicable to the entirety of a biomolecular or other chemical system, and which thus may provide additional guidance for molecular design. For example, it might highlight parts of a ligand whose local free energy rises on binding, thus suggesting where modifications could improve affinity. Starting from classical statistical thermodynamics, we derive structural decompositions that assign energy and entropy to individual atoms or to larger chemical components, such as amino acid residues, and spatial decompositions that define continuously varying thermodynamic densities throughout the system. The potential energy is decomposed via the multibody expansion, and the entropy via the mutual information expansion. The resulting thermodynamic densities satisfy key desiderata: their spatial integrals yield the correct total thermodynamic quantities, the densities vanish where the atomic number density is zero, and all entropy terms above first order go to zero in the absence of correlation. The entropy decomposition in GTM theory is closely related to that of IST, but it is simpler, largely because it expresses the entropy in terms of normalized probability density functions instead of

non-normalized correlation functions. We show that, while GTM theory is formally exact for any number of particles, N, IST is not. The unified framework presented here enables thermodynamic mapping of solute and solvent alike and is expected to support a range of applications, including in structure-based drug design, protein design, the analysis of allostery, and materials science. The use of GTM theory to gain insight into protein-ligand binding is illustrated here with an initial case study.

Keywords

Drug design, Molecular dynamics, Entropy, Free Energy

A Generalized Theory for the Structural and Spatial Mapping of Energy, Entropy, and Free Energy

Michael K. Gilson[*,1], Joe Cruz[2], Kunhuan Liu[1], Samrat Lohar[2], Helmut Carter[2], Daniel R. Roe[3], Tom Kurtzman[*,2]

September 4, 2026

1. Department of Pharmaceutical Sciences, Skaggs School of Pharmacy and Pharmaceutical Sciences, University of California San Diego, La Jolla, CA 92093, USA.

2. PhD Programs in Chemistry, Biochemistry, and Biology, The Graduate Center of the City University of New York, New York, 10016, USA; Department of Chemistry, Lehman College, The City University of New York, Bronx, New York, 10468, USA.

3. Laboratory of Computational Biology, National Heart, Lung, and Blood Institute, National Institutes of Health, Bethesda, Maryland, 20892, USA

* To whom correspondence should be addressed. mgilson@ucsd.edu, simpleliquid@gmail.com

Abstract

Systems in which the free energy density is nonuniform in space are familiar; the surface tension of a water droplet and the surface energy of a solid are good examples. Some such cases can be treated with prior theory, notably inhomogeneous solvation theory (IST), but IST is applicable only to liquids. Despite this limitation, IST has proven useful as a guide to the design of ligands to bind a targeted protein, based on the idea that ligands which displace high free energy water will tend to bind more tightly, other things being equal. Here, we present Generalized Thermodynamic Mapping (GTM) theory, a more general theory that is applicable to the entirety of a biomolecular or other chemical system, and which thus may provide additional guidance for molecular design. For example, it might highlight parts of a ligand whose local free energy rises on binding, thus suggesting where modifications could improve affinity. Starting from classical statistical thermodynamics, we derive structural decompositions that assign energy and entropy to individual atoms or to larger chemical components, such as amino acid residues, and spatial decompositions that define continuously varying thermodynamic densities throughout the system. The potential energy is decomposed via the multibody expansion, and the entropy via the mutual information expansion. The resulting thermodynamic densities satisfy key desiderata: their spatial integrals yield the correct total thermodynamic quantities, the densities vanish where the atomic number density is zero, and all entropy terms above first order go to zero in the absence of correlation. The entropy decomposition in GTM theory is closely related to that of IST, but it is simpler, largely because it expresses the entropy in terms of normalized probability density functions instead of non-normalized correlation functions. We show that, while GTM theory is formally exact for any number of particles, N, IST is not. The unified framework presented here enables thermodynamic mapping of solute and solvent alike and is expected to support a range of applications, including in structure-based drug design, protein design, the analysis of allostery, and materials science. The use of GTM theory to gain insight into protein-ligand binding is illustrated here with an initial case study.

1 Introduction

A chemical system at equilibrium does not, in general, have a uniform spatial distribution of free energy, energy, or entropy. For example, the surface tension of a water droplet, which is defined as the free energy per unit area of the surface, corresponds at the microscopic level to an elevated free energy per unit volume in the region of space where the mass density grades from its bulk liquid value to its vapor value. In addition, given that the free energy comprises an energetic component and an entropy component, there must be corresponding position-dependent energy and entropy densities. Solids also can have spatially varying thermodynamics, such as grain boundary energies that deviate from the bulk energy,[1] and spatially varying elastic energy densities in objects under nonuniform mechanical stress. However, there has not, so far, been a unified and rigorous theory for analyzing and computing spatial or structural variations in thermodynamics within a general system of interest.

Importantly, there is already well-developed theory for spatially mapping solvation thermodynamics, namely inhomogeneous solvation theory (IST).[2,3] IST provides expressions for position-dependent thermodynamic densities for the special case of a fluid in the context of a rigid solute molecule. These expressions can be numerically evaluated through analysis of molecular simulations, and software implementing IST analysis of simulations is used for structure-based drug design.[4–8] The rationale for this application is that a ligand may gain affinity for a protein by displacing binding site water that has a high free energy density and hence is thermodynamically unfavorable.[9–12] Binding of a ligand returns this water to the bulk, leading to an increment in binding affinity.

Given the utility of IST, we anticipate that a *generalized* thermodynamic mapping theory (GTM theory), i.e., one that is rigorous and smoothly applicable across all components of systems made up of fluids and/or solids, will be even more useful, providing a theoretical basis for reasoning about such systems and enabling the development of tools to gain mechanistic insight from molecular simulations. For example, explicit solvent free energy methods[13–18] are widely used to predict protein-ligand binding free energies in the pharmaceutical and biotechnology industries, but neither explain why one ligand binds better than another nor tell how to modify an initial ligand to generate a new ligand with greater affinity. A comprehensive decomposition of the change in free energy on binding could provide information on which parts of a ligand contribute favorably to the computed binding affinity and therefore should be retained; which parts oppose binding and therefore should be modified; and which parts of the binding pocket could be used to generate new interactions that favor binding. Note that some applications may be best served by a *spatial* mapping of thermodynamic densities, like that provided by IST, though now extended to the protein and ligand themselves; but others may benefit instead from a *structural* decomposition, in which thermodynamic contributions are assigned to atoms or other molecular components.

The ability to spatially or structurally map thermodynamic quantities also promises to be useful in understanding and predicting allostery, which is of critical biomedical importance in phenomena ranging from activation of GPCRs, to regulation of metabolic enzymes, to the transduction of chemical energy into mechanical energy by molecular motors. In one view, the binding of an allosteric effector generates a rise in local free energy around the binding site, which, in turn, drives a distal allosteric change that relaxes the initial, local, free energy rise. This view fits intuitive explanations common in the literature based on concepts of mechanical stress and strain and local energy storage and release.[19–22] However, our explorations of mechanical stress in proteins,[23] including unpublished work, have made it clear that a formal accounting of stress is not particularly informative for proteins. This is because the free energy stored in a protein structure does not vary linearly with stress, as in a simple elastic solid. Instead, the energy landscape has many local energy wells at various energy levels, so a protein can be under little mean stress while in a high-lying local energy minimum. A thermodynamic mapping which accounts for this complexity should be informative regarding energy storage and relaxation in complex molecular systems with nonlinear stress/strain relationships.

In prior work, we used the mutual information expansion (MIE) of entropy to estimate

changes in the configurational entropy of a protein and ligand on binding.[24] More recently, we demonstrated that the MIE can also be used as the basis of an IST-like mapping of the entropy of a fluid.[25] Here, building on these advances, we define a rigorously founded GTM theory in which the entropy is handled entirely via the MIE. This fills a longstanding gap in the literature, namely the absence of a theory capable of mapping thermodynamic quantities across a wide range of chemical systems. The mappings are derived from the basic equations of classical statistical thermodynamics, and their sums over atoms (for structural mappings) and spatial integrals (for spatial mappings) converge asymptotically to the correct system properties in the appropriate multibody limits. In particular, the densities satisfy basic desiderata[25] that the spatial integral of the free energy density over the entire system should give the correct system free energy, that the free energy density should go to zero where the spatial number density of atoms goes to zero, and that all entropy terms above first order should go to zero in the absence of correlation (i.e., in the limit of an ideal gas).

This paper derives and explains the theory, elaborates its connection with IST, and provides a case study that illustrate mappings of protein-ligand binding thermodynamics. Section 2 starts with an overview of the approach and a detailed definition of the physical system and coordinate system. It then presents derivations of atom-based structural and spatial mappings of the mean potential energy and entropy, followed by mappings based on molecules and more general chemical components, such as protein residues. Section 3 details the relationship of the present mappings to the solvent energy and entropy densities provided by IST, and Section 4 provides an illustrative application to protein-ligand binding. Finally, the Discussion considers implications and outlines future research directions based on this new theoretical foundation.

2 General Thermodynamic Mapping Theory (GTM theory)

2.1 Overview of General Thermodynamic Mapping Theory

We use the fact that both the potential energy and the entropy of a chemical system can be written without approximation as series expansions. Thus, any potential energy function can be expressed as a multibody expansion,[25] and the entropy of a multivariable system can be expressed in terms of the mutual information expansion (MIE).[26–28] We may therefore, as diagrammed in Figure 1, decompose the potential energy across bodies – typically atoms – by assigning to atom i its full one-body energy, half of its two-body energy, etc. Analogously, atom i may be assigned its entire marginal entropy, minus one half of its pairwise mutual information with all other atoms, etc. We use these expansions to derive expressions for structural decompositions, which assign energy and entropy contributions to individual atoms or larger structural elements, and for spatial mappings, which define position-dependent energy and entropy densities. In practice, the entropy expansion must typically be truncated at low order (e.g. second or third), because converging higher order terms can become computationally intractable. However, the potential energy expansion for today's commonly used force fields terminates at second order for nonbonded interactions (typically Lennard-Jones and electrostatic)

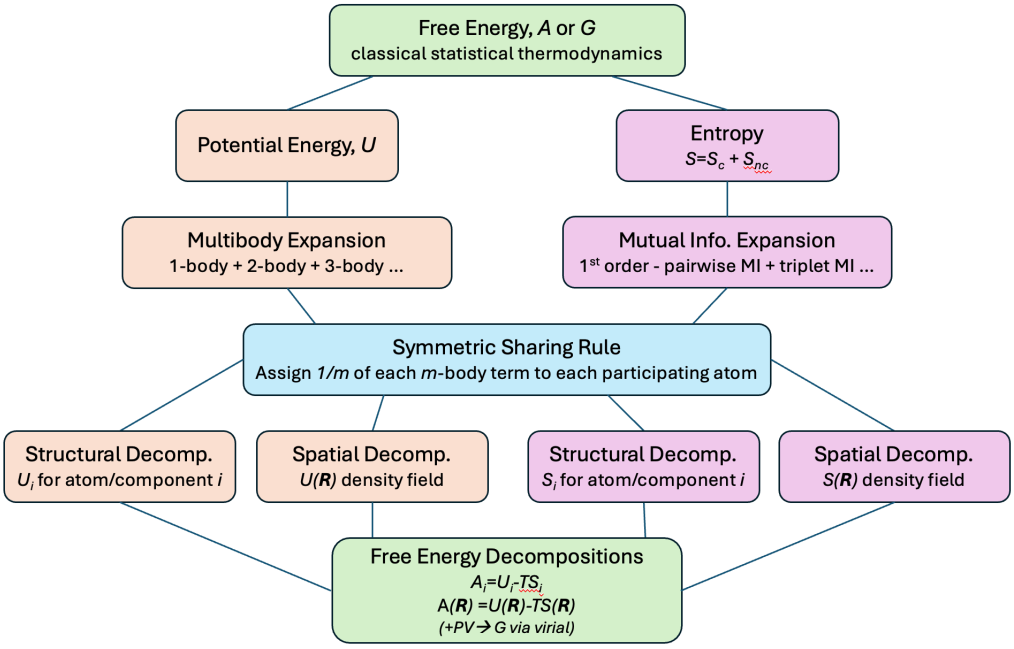

Figure 1: Structure of GTM theory. Within classical thermodynamics, the free energy is split into the mean potential energy and the entropy (configurational and non-configurational) contributions. Expression of energy in terms of a multibody expansion and entropy in terms of the mutual information expansion allows each contribution to be decomposed structurally (i.e., by atom or chemical component) and spatially (i.e., as thermodynamic densities). The decomposed energy and entropy can then be reassembled to provide structural and spatial decompositions of the free energy. The bottom rectangle lists the Helmholtz free energy, A, while noting that the pressure-volume product, PV, when expressed in terms of the virial, can also be decomposed, allowing full decomposition of the Gibbs free energy as well. Symbols used here are defined in Table 1 and the text.

and at fourth order for bonded interactions (i.e. bond-stretch, bond-angle, and torsion), and its decompositions can be evaluated in full.

2.2 System Definition

We consider a flexible solute, such as an organic compound or a protein, immersed in a pure solvent, such as hexane or water, where the entire system of N atoms is contained in a volume V at temperature T and pressure P. The thermodynamic properties to be mapped are the mean potential energy, U, the entropy, S, the Helmholtz free energy, A, and the Gibbs free energy, G. Note that we remain within the classical approximation of statistical thermodynamics.[29]

Before proceeding further, we switch from a lab-frame coordinate system to an internal Cartesian coordinate system, i.e., one rooted in the frame of reference of the solute (Figure 2). If we used a laboratory frame of reference, local variations in thermodynamic densities around the solute would be averaged over the entire system volume due to translation of the solute in the lab frame, and thus would be uniform over the volume. Lab-frame rotations on their own would similarly smear variations in thermodynamic density and lead to relatively uninteresting radially symmetric densities. Such results

would not be wrong, but they would be uninformative. One way to set up such a coordinate system is to choose one solute atom, i, as the origin of coordinates; choose a second solute atom, j, and define the x-axis in terms of the unit vector from atom i to atom j; choose a third atom, k, and define the y-axis in terms of the unit vector starting at atom i, in the plane defined by atoms i, j, and k, and orthogonal to the new x-axis; and define the z axis as vector starting at atom i and extending orthogonally to both the x- and y-axes. With this definition, the coordinates of atom i are always $\mathbf{r}_i = (0, 0, 0)$, those of atom j are always $\mathbf{r}_j = (x_j, 0, 0)$, and those of atom k are always $\mathbf{r}_k = (x_k, y_k, 0)$, where the six zeroes associated with the three root atoms correspond to the eliminated degrees of freedom (or, more properly, to the external degrees of freedom of the solute). For convenience, we still write the coordinates of all N atoms as $\mathbf{r}^N = (\mathbf{r}_1, \mathbf{r}_2, \ldots, \mathbf{r}_N)$. Note that, to avoid a situation where the internal coordinates become numerically unstable because atoms i, j, k are nearly collinear, it is helpful to choose i, j, k as three sp3 or sp2 hybridized atoms in bonding sequence, so that the i, j, k angle remains far from zero. (The condition of exact collinearity does not pose a substantive theoretical problem because the phase space volume associated with this singularity is infinitesimal.) Details of the present coordinate change are available in the "Anchored Coordinates" part of the Appendix of a prior publication.[30] One could, alternatively, use the principle moments of inertia of the molecule to define a solute-based coordinate frame. However, this might be problematic for a flexible solute, as the principal moments of inertia are conformation-dependent, so conformational fluctuations may lead to fluctuations in the orientation and ordering of the resulting coordinate axes.

We have chosen to develop GTM theory in this solute-based, Cartesian coordinate system in order to optimize the simplicity and clarity of the equations and thus to best explicate the theory. However, when applying GTM theory to anything other than a rigid solute or a solid, it will typically be preferable to make the straightforward transformation to bond-angle-torsion (BAT) coordinates with phase angles, as done in our prior applications of the MIE to proteins.[28] Although BAT coordinates make for more complicated equations, due to the introduction of a Jacobian determinant and the use of different symbols for bond-length, bond-angle, and torsion-angle variables, they have the practical advantage of reducing the degree of correlations among variables and thus the amount of sampling needed to achieve a given level of numerical convergence.

We now summarize important aspects of the notation used here, while Table 1 defines additional symbols used in this paper. The total mean potential energy U and entropy S of the system are either mapped into atomic contributions, U_i and S_i for atom i, or to spatial densities, $U(\mathbf{R})$ and $S(\mathbf{R})$, at location $\mathbf{R}$ in the solute-based reference frame. In Section 2.6, we distinguish between the positional (i.e., translational) coordinates $\mathbf{r}_a$ and the combined internal and orientational coordinates $\mathbf{q}_a$ of a given molecule (e.g., a water molecule) or chemical component (e.g., a protein residue) a.

The probability density function (PDF) over all atomic coordinates is $p(\mathbf{r}^N)$, and marginal probability density functions for e.g. single atoms and pairs of atoms, are

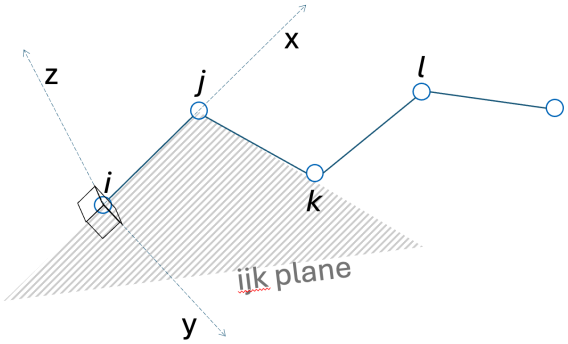

Figure 2: Diagram of one way to define a Cartesian coordinate system in the frame of reference of the solute. Atoms indexed i, j, k define the coordinate system, with the origin at atom i, x-axis lying along the $i - j$ bond, the y-axis orthogonal to the x-axis and in the i, j, k plane, and the z-axis orthogonal to both the x- and y-axes.

given by:

$$p(\mathbf{r}_i) = \int p(\mathbf{r}^N) \prod_{k \neq i}^{N} d\mathbf{r}_k$$
$$p(\mathbf{r}_i, \mathbf{r}_j) = \int p(\mathbf{r}^N) \prod_{k \neq i,j}^{N} d\mathbf{r}_k \tag{1}$$

Here $\prod_{k\neq i}^{N}$ indicates a product where index k ranges from 1 to N except that $k = i$ is omitted, and $\prod_{k\neq i,j}^{N}$ is the same except that both $k = i$ and $k = j$ are omitted. In constructing GTM theory, we build on the Irving-Kirkwood formalism,[31] which uses delta functions to define continuously varying spatial densities. For example, the mass density in space, $M(\mathbf{R})$, would be written as follows in terms of atomic masses m_i, PDFs $p(\mathbf{r}_i)$, and positions, $\mathbf{r}_i$:

$$M(\mathbf{R}) = \int \sum_{i=1}^{N} \left[\delta(\mathbf{R} - \mathbf{r}_i)\, m_i\, p(\mathbf{r}_i)\right] d\mathbf{r}_i \tag{2}$$

The delta functions pick out the contribution of each atom, i, at location $\mathbf{R}$. However, when comparing GTM theory with IST in Section 3, we revert to the simpler but less general formalism typically used to express IST.

	Coordinates and Counts
$\mathbf{r}_i$	Cartesian coordinates (x, y, z) of atom i
$\mathbf{r}^N$	$(\mathbf{r}_1, \mathbf{r}_2, \ldots, \mathbf{r}_N)$, all N sets of atomic coordinates in a given system configuration.
$\mathbf{R}$	Cartesian coordinates (x, y, z); used for thermodynamic densities
$\mathbf{q}$	combined orientational and internal coordinates of a molecule or other chemical component
$\mathbf{p}^N$	Momenta of all N atoms
$\mathbf{p}_i$	Momentum of atom i
N_{perm}	Number of permutations among all indistinguishable atoms
n_l	Number of indistinguishable atoms in group l
	Distribution and Correlation Functions
$p(\mathbf{r}^N, \mathbf{p}^N)$	Normalized probability distribution function (PDF) over all spatial and momentum coordinates
$P(\mathbf{r}^N, \mathbf{p}^N)$	Non-normalized distribution function defined in Eq 12
$p(\mathbf{r}^N)$	Normalized PDF over Cartesian coordinates of all N atoms
$p(\mathbf{r}_i)$	Normalized marginal PDF of atom i as a function of its atomic coordinates, $\mathbf{r}_i$
$p(\mathbf{r}, \mathbf{r'})$	Normalized joint PDF of atoms i, j as a function of their respective positions, $\mathbf{r}, \mathbf{r}'$
$p(\mathbf{q}_a \vert \mathbf{r}_a)$	PDF of orientational and internal coordinates $\mathbf{q}$ of chemical component a conditioned on its being located at $\mathbf{r}$
$g(\mathbf{r})$	One-body solvent correlation function, as used in IST
$g(\mathbf{r}, \mathbf{r'})$	Two-body solvent correlation function, as used in IST
ρ	Number density
	Energy
U	Mean potential energy of the system
U($\mathbf{R}$)	Potential energy density at $\mathbf{R}$
$U(\mathbf{r}^N)$	Instantaneous potential energy of configuration $\mathbf{r}^N$
$u_i(\mathbf{r}_i)$	One-body potential energy term for atom i as a function of $\mathbf{r}_i$
$u_{ij}(\mathbf{r}_i, \mathbf{r}_j)$	Two-body potential energy term for atoms i, j as a function of $\mathbf{r}_i, \mathbf{r}_j$
$U_i(\mathbf{r}^N)$	Potential energy assigned to atom i for a given system configuration, $\mathbf{r}^N$
U_i	Mean potential energy assigned to atom i
$U_i(\mathbf{R})$	Mean potential energy density at $\mathbf{R}$ contributed by atom i
U_a	Mean potential energy associated with chemical component a
$U_a(\mathbf{R})$	Mean potential energy density at $\mathbf{R}$ contributed by chemical component a
	Entropy
S	Entropy of the system
S_c	Configurational entropy of the system
$S_c(\mathbf{R})$	Configurational entropy density at $\mathbf{R}$
$S_{c,i}(\mathbf{R})$	Configurational entropy density of atom i at $\mathbf{R}$
$S_{c,i}$	Configurational entropy of atom i
S_{nc}	Nonconfigurational entropy of the system
$S_{nc,i}$	Nonconfigurational entropy of atom i
$S_{nc}(\mathbf{R})$	Nonconfigurational entropy density at $\mathbf{R}$
$S_{nc,i}(\mathbf{R})$	Nonconfigurational entropy density of atom i at $\mathbf{R}$
S($\mathbf{R}$)	Entropy density at $\mathbf{R}$
$S_c^{(1)}$	First order contribution to (and first-order estimate of) the configurational entropy
$S_{c,i}^{(1)}$	First order contribution to (and first-order estimate of) the configurational entropy associated with atom i
$S_c^{(2)}$	Second order estimate of the configurational entropy
I_{ij}	Mutual information between atoms i and j
$I_i^{(2)}$	Pairwise mutual information associated with atom i
$I_{ij}(\mathbf{R})$	Density of mutual information between atoms i and j and associated with atom i, at $\mathbf{R}$.
$S^{(1)}(\mathbf{R})$	First order contribution to (and estimate of) configurational entropy at $\mathbf{R}$
$I^{(2)}(\mathbf{R})$	Pairwise mutual information density at $\mathbf{R}$
$S_a^q(\mathbf{R})$	Density of the orientational/internal entropy of component a conditioned on component a being located at $\mathbf{R}$
S_{ig}	Entropy of an ideal gas
$S_{IST}^{(2)}$	Second order estimate of entropy from IST
$S_{IST}^{(1)}(\mathbf{r})$	First order estimate of entropy density from IST at $\mathbf{r}$
$S_{IST}^{(2)}(\mathbf{r})$	Second order estimate of entropy density from IST at $\mathbf{r}$
	Free Energy
A	Helmholtz free energy of the system
A_i	Helmholtz free energy assigned to atom i
$A(\mathbf{R})$	Helmholtz free energy density as a function of position
G	Gibbs free energy of the system
G_i	Gibbs free energy assigned to atom i
$G(\mathbf{R})$	Gibbs free energy density as a function of position
$\mathcal{W}(\mathbf{r}^N)$	Virial of the system in configuration $\mathbf{r}^N$
$\mathcal{W}_i(\mathbf{r}^N)$	Contribution of atom i to the virial, for system configuration $\mathbf{r}^N$
$(PV)_i$	Contribution of atom i to the pressure-volume product

Table 1: Definitions of selected symbols used in this paper.

2.3 Mapping the Potential Energy

The mean potential energy of the entire system is given by

$$U = \int p(\mathbf{r}^N) U(\mathbf{r}^N) d\mathbf{r}^N \tag{3}$$

For example, in the canonical ensemble,

$$p(\mathbf{r}^N) = \frac{e^{-\beta U(\mathbf{r}^N)}}{Z} \tag{4}$$

$$Z = \int e^{-\beta U(\mathbf{r}^N)} d\mathbf{r}^N \tag{5}$$

where $U(\mathbf{r}^N)$ is the potential energy as a function of the atomic coordinates, $\mathbf{r}^N$; $p(\mathbf{r}^N)$ is the PDF over all atomic coordinates and is given by the Boltzmann distribution defined in Equations 4 and 5; Z is the configuration integral, and $\beta = 1/k_B T$, with k_B the Boltzmann constant and T the absolute temperature. Note that, to maintain a compact notation, we consider an energy term without an argument, such as U or U_i, to represent a thermodynamic average, while an energy term with an argument, such as $U(\mathbf{r}^N)$ or $U_i(\mathbf{r}^N)$, represents an instantaneous value of the energy for the configuration, here $\mathbf{r}^N$.

2.3.1 Structural Mapping of the Potential Energy

Here, we derive a decomposition, or mapping, of the mean potential energy, U, to individual atoms, while Section 2.6 provides a decomposition by chemical components comprising multiple atoms, such as entire solvent molecules or the separate residues of a protein. We begin with the multibody expansion of the instantaneous potential energy, where a "body" is an atom,

$$U(\mathbf{r}^N) = \sum_{i=1}^{N} u_i(\mathbf{r}_i) + \sum_{i=1}^{N}\sum_{j>i}^{N} u_{ij}(\mathbf{r}_i, \mathbf{r}_j) + \sum_{i=1}^{N}\sum_{j>i}^{N}\sum_{k>j}^{N} u_{ijk}(\mathbf{r}_i, \mathbf{r}_j, \mathbf{r}_k) + \dots \tag{6}$$

where i, j, k index atoms; $u_i(\mathbf{r}_i)$, $u_{ij}(\mathbf{r}_i, \mathbf{r}_j)$, and $u_{ijk}(\mathbf{r}_i, \mathbf{r}_j, \mathbf{r}_k)$ are the 1-body, 2-body, and 3-body energy contributions associated with atom i, atom pair i, j, and atomic triplet i, j, k, respectively; and the ellipsis indicates the possibility of 4-body and higher terms. In a prior paper,[25] we used ϕ rather than u in the multibody expansion; we change notation here for simplicity and for consistency with the broader literature. Note that these sums run over all atoms of both the solute and solvent, so they include the interactions of the solute atoms with the solvent. Therefore, the one-body term is expected to be nonzero only in the presence of an external field, whereas in IST, which focuses on the solvent, the first order term reflects the interactions of the solvent with the solute.

We now define the potential energy associated with any atom, i, for a given configuration, $\mathbf{r}^N$, as:

$$U_i(\mathbf{r}^N) = u_i(\mathbf{r}_i) + \frac{1}{2}\sum_{j\neq i}^{N} u_{ij}(\mathbf{r}_i, \mathbf{r}_j) + \frac{1}{3}\sum_{j\neq i}^{N}\sum_{\substack{k\neq i \\ k>j}}^{N} u_{ijk}(\mathbf{r}_i, \mathbf{r}_j, \mathbf{r}_k) + \dots \tag{7}$$

This expression assigns all of atom i's interaction with any external field to atom i alone; it assigns one half of all of atom i's interactions with other atoms j to atom i,

leaving the other half to be assigned to atoms j, and it assigns one third of the three-body interactions that involve atom i to atom i. For example, for a four-atom system, atom 1 is assigned the following energy, to third order:

$$\begin{aligned} U_1(\mathbf{r}^N) = u_1(\mathbf{r}_1) &+ \frac{1}{2}\left[u_{12}(\mathbf{r}_1,\mathbf{r}_2) + u_{13}(\mathbf{r}_1,\mathbf{r}_3) + u_{14}(\mathbf{r}_1,\mathbf{r}_4)\right] \\ &+ \frac{1}{3}\left[\, u_{123}(\mathbf{r}_1,\mathbf{r}_2,\mathbf{r}_3) + u_{134}(\mathbf{r}_1,\mathbf{r}_3,\mathbf{r}_4) + \right. \\ &\left. + u_{124}(\mathbf{r}_1,\mathbf{r}_2,\mathbf{r}_4)\,\right] \end{aligned}$$

The elided higher order terms of the multibody potential make analogous contributions to atom i's potential energy. The total system potential energy, $U(\mathbf{r}^N)$, is, by construction, the sum of the atomistic potential energies over all solute and solvent atoms:

$$U(\mathbf{r}^N) = \sum_{i=1}^{N} U_i(\mathbf{r}^N) \tag{8}$$

Therefore, Equation 7 provides a well-defined mapping of the total potential energy to individual atoms for a given configuration, and averaging over configurations gives the contribution, U_i, of each atom to the mean potential energy of the system:

$$\begin{aligned} U &= \sum_{i=1}^{N} U_i \\ U_i &= \int p(\mathbf{r}^N) U_i(\mathbf{r}^N) d\mathbf{r}^N \\ &= \int p(\mathbf{r}_i) u_i(\mathbf{r}_i) d\mathbf{r}_i + \frac{1}{2}\sum_{j\neq i}^{N} \int p(\mathbf{r}_i,\mathbf{r}_j) u_{ij}(\mathbf{r}_i,\mathbf{r}_j) d\mathbf{r}_i d\mathbf{r}_j \\ &+ \frac{1}{3}\sum_{j\neq i}^{N}\sum_{\substack{k\neq i \\ k>j}}^{N} \int p(\mathbf{r}_i,\mathbf{r}_j,\mathbf{r}_k) u_{ijk}(\mathbf{r}_i,\mathbf{r}_j,\mathbf{r}_k) d\mathbf{r}_i d\mathbf{r}_j d\mathbf{r}_k + \ldots \end{aligned} \tag{9}$$

where we have used the fact that $\int p(\mathbf{r}^N) \prod_{k\neq i}^{N} d\mathbf{r}_k = p(\mathbf{r}_i)$ to write $\int p(\mathbf{r}^N) u_i(\mathbf{r}_i) d\mathbf{r}^N = \int p(\mathbf{r}_i) u_i(\mathbf{r}_i) d\mathbf{r}_i$, and similarly for the higher order terms.

2.3.2 Spatial Mapping of the Potential Energy Density

This structural decomposition of the energy is expected to be useful for the solute, where chemically distinct atoms make distinct, interpretable, contributions to U. In contrast, because the solvent molecules are identical to each other and share identical probability density functions, they will be assigned identical mean energies. For example, if the solvent is water, then every water oxygen will be assigned the same mean energy, U_O, and every hydrogen atom will be assigned the same mean energy, U_H, so the total mean energy of each water, $U_w = U_O + 2U_H$, will be the same for every water molecule in the system, making such an analysis relatively uninformative. A spatial mapping of the potential energy is more useful in this setting.[32,33] In GTM theory, a spatial mapping

of mean potential energy is constructed by inserting the delta-function $\delta(\mathbf{R}-\mathbf{r}_i)$ into the integrals of Equation 9 to pick out the mean energy of each atom when it is at $\mathbf{R}$, yielding $U_i(\mathbf{R})$, and summing $U_i(\mathbf{R})$ over atoms i to obtain $U(\mathbf{R})$:

$$\begin{aligned}
U(\mathbf{R}) &= \sum_{i=1}^{N} U_i(\mathbf{R}) \\
U_i(\mathbf{R}) &= \int \delta(\mathbf{R}-\mathbf{r}_i) p(\mathbf{r}^N) U_i(\mathbf{r}^N) d\mathbf{r}^N \\
&= \int \delta(\mathbf{R}-\mathbf{r}_i) p(\mathbf{r}_i) u_i(\mathbf{r}_i) d\mathbf{r}_i + \frac{1}{2}\sum_{j\neq i}^{N} \int \delta(\mathbf{R}-\mathbf{r}_i) p(\mathbf{r}_i,\mathbf{r}_j) u_{ij}(\mathbf{r}_i,\mathbf{r}_j) d\mathbf{r}_i d\mathbf{r}_j \\
&+ \frac{1}{3}\sum_{j\neq i}^{N}\sum_{\substack{k\neq i \\ k>j}}^{N} \int \delta(\mathbf{R}-\mathbf{r}_i) p(\mathbf{r}_i,\mathbf{r}_j,\mathbf{r}_k) u_{ijk}(\mathbf{r}_i,\mathbf{r}_j,\mathbf{r}_k) d\mathbf{r}_i d\mathbf{r}_j d\mathbf{r}_k \;+\; \ldots
\end{aligned} \tag{10}$$

With these definitions, it is clear that

$$\begin{aligned}
U_i &= \int U_i(\mathbf{R}) d\mathbf{R} \\
U &= \int U(\mathbf{R}) d\mathbf{R}
\end{aligned} \tag{11}$$

Thus, our definition of the potential energy density satisfies the desideratum that its integral over the system volume equals the mean potential energy.

2.4 Mapping the Entropy

We start with Wallace's expression for the total entropy[34] in terms of the following non-normalized distribution function

$$P(\mathbf{r}^N,\mathbf{p}^N) = \frac{e^{-\beta H(\mathbf{r}^N,\mathbf{p}^N)}}{\frac{1}{h^{3N}N_{perm}}\int e^{-\beta H(\mathbf{r}^N,\mathbf{p}^N)} d\mathbf{r}^N d\mathbf{p}^N} \tag{12}$$

which should be distinguished from the normalized PDF

$$p(\mathbf{r}^N,\mathbf{p}^N) = \frac{e^{-\beta H(\mathbf{r}^N,\mathbf{p}^N)}}{\int e^{-\beta H(\mathbf{r}^N,\mathbf{p}^N)} d\mathbf{r}^N d\mathbf{p}^N} \tag{13}$$

where $H(\mathbf{r}^N,\mathbf{p}^N)$ is the total energy (kinetic and potential) as a function of spatial coordinates $\mathbf{r}^N$ and momenta $\mathbf{p}^N$, and h is Planck's constant. Because i ranges over both solute and solvent atoms, only certain subsets of particles are indistinguishable, so we have replaced $N!$ by N_{perm}, the number of possible permutations of all indistinguishable atoms. If there are n groups l of indistinguishable atoms, each with n_l atoms, such that $\sum_{l=1}^{n} n_l = N$, then $N_{perm} = \prod_{l=1}^{n} n_l!$, so, for example, $N_{perm} = 1$ if all atoms are distinct, and $N_{perm} = N!$ if all atoms are identical.

Following Wallace, we write the entropy as

$$\begin{aligned} S &= -\frac{k_B}{h^{3N} N_{perm}} \int P(\mathbf{r}^N, \mathbf{p}^N) \ln P(\mathbf{r}^N, \mathbf{p}^N) d\mathbf{r}^N d\mathbf{p}^N \\ &= -k_B \int p(\mathbf{r}^N, \mathbf{p}^N) \left[\ln p(\mathbf{r}^N, \mathbf{p}^N) + \ln(h^{3N} N_{perm}) \right] d\mathbf{r}^N d\mathbf{p}^N \\ &= S_c + S_{nc} \\ S_c &= -k_B \int p(\mathbf{r}^N) \ln p(\mathbf{r}^N) d\mathbf{r}^N \\ S_{nc} &= -k_B \sum_{i=1}^{N} \left[\int p(\mathbf{p}_i) \ln p(\mathbf{p}_i) d\mathbf{p}_i \right] - k_B \ln(h^{3N} N_{perm}) \end{aligned} \tag{14}$$

where we have factorized the integral by using the fact that, in the classical approximation and at equilibrium, momenta are statistically independent of position and of each other, so $p(\mathbf{r}^N, \mathbf{p}^N) = p(\mathbf{r}^N) \prod_i p(\mathbf{p}_i)$.

Here S_c is the Gibbs-Shannon configurational entropy, and S_{nc}, the non-configurational entropy, contains the momentum entropy, the indistinguishability correction, and a term involving Planck's constant which cancels the units of the probability density functions over position and momentum in the other logarithmic terms. The non-configurational entropy is unaffected by changes in $p(\mathbf{r}^N)$ at constant T and N, and hence is of little interest in many applications, so it is often set aside.[32,33,35] We include S_{nc} nonetheless, as it depends on temperature and composition, and there are cases where these are not constant. Including it also facilitates comparisons with prior papers that used comparisons with the Sackur-Tetrode equation as a test of validity.[34,36]

2.4.1 Structural Mapping of the Entropy

We consider S_{nc} and then S_c. To decompose S_{nc}, we use the well-known fact that, in classical statistical thermodynamics, the PDFs of the three momentum components of each atom are statistically independent. This allows us to factorize $p(\mathbf{p}_i)$ into three identical Gaussian distributions, for which the entropy can be written analytically:

$$p(\mathbf{p}_i) = p(\mathbf{p}_{ix}) p(\mathbf{p}_{iy}) p(\mathbf{p}_{iz}) = \left[\frac{e^{-\frac{p_x^2}{2mk_BT}}}{\int e^{-\frac{p_x^2}{2mk_BT}} dp_x} \right]^3$$

$$-k_B \int p(\mathbf{p}_i) \ln p(\mathbf{p}_i) d\mathbf{p}_i = 3\frac{k_B}{2} \left[1 + \ln(2\pi m k_B T) \right] = 3k_B \left[\frac{1}{2} - \ln \Lambda_i + \ln h \right] \tag{15}$$

where $\mathbf{p}_{ix}, \mathbf{p}_{iy}, \mathbf{p}_{iz}$ are the three momentum components of atom i, and $\Lambda_i = \frac{h}{\sqrt{2\pi m_i k_B T}}$ is the de Broglie wavelength of atom i with mass m_i. Thus, we may write the non-configurational entropy as

$$\begin{aligned} S_{nc} &= \frac{3Nk_B}{2} - k_B \sum_{i=1}^{N} \ln \Lambda_i^3 + 3Nk_B \ln h - 3Nk_B \ln h - k_B \ln N_{perm} \\ &= \frac{3Nk_B}{2} - k_B \sum_{i=1}^{N} \ln \Lambda_i^3 - k_B \ln N_{perm} \end{aligned} \tag{16}$$

This allows a natural decomposition of the non-configurational entropy given in Equation 16 by atoms, i:

$$\begin{aligned} S_{nc} &= \sum_{i=1}^{N} S_{nc,i} \\ S_{nc,i} &= k_B \left[\frac{3}{2} - \ln \Lambda_i^3 - \frac{\ln n_{l(i)}!}{n_{l(i)}} \right] \end{aligned} \tag{17}$$

where we have introduced $l(i)$, a function which returns the index l of the indistinguishability group that i belongs to. In the limit of large N and hence n_l, application of Stirling's approximation gives

$$S_{nc,i} = k_B \left[\frac{5}{2} - \ln \Lambda_i^3 - \ln n_{l(i)} \right] \tag{18}$$

The MIE allows the configurational entropy to be written as a sum of 1-atom, 2-atom, 3-atom, etc, terms:

$$S_c = \sum_{i=1}^{N} S_{c,i}^{(1)} - \sum_{i=1}^{N} \sum_{j>i}^{N} I_{ij} + \sum_{i=1}^{N} \sum_{j>i}^{N} \sum_{k>j}^{N} I_{ijk} \ldots \tag{19}$$

where, for simplicity, and since there are no non-configurational mutual information terms, we have omitted a "c" subscript from the mutual information contributions. The 1-body (i.e., one-atom) configurational entropies are

$$S_{c,i}^{(1)} = -k_B \int p(\mathbf{r}_i) \ln p(\mathbf{r}_i) d\mathbf{r}_i \tag{20}$$

the 2-body mutual information terms have the general form $I_{ij} = S_i + S_j - S_{ij}$ and are given here by

$$\begin{aligned} I_{ij} &= -k_B \int p(\mathbf{r}_i) \ln p(\mathbf{r}_i) d\mathbf{r}_i - k_B \int p(\mathbf{r}_j) \ln p(\mathbf{r}_j) d\mathbf{r}_j \\ &+ k_B \int p(\mathbf{r}_i, \mathbf{r}_j) \ln p(\mathbf{r}_i, \mathbf{r}_j) d\mathbf{r}_i d\mathbf{r}_j \end{aligned} \tag{21}$$

and the 3-atom terms take the following form

$$\begin{aligned} I_{ijk} &= -k_B \int p(\mathbf{r}_i, \mathbf{r}_j, \mathbf{r}_k) \ln p(\mathbf{r}_i, \mathbf{r}_j, \mathbf{r}_k) d\mathbf{r}_i d\mathbf{r}_j d\mathbf{r}_k + k_B \int p(\mathbf{r}_i, \mathbf{r}_j) \ln p(\mathbf{r}_i, \mathbf{r}_j) d\mathbf{r}_i d\mathbf{r}_j \\ &+ k_b \int p(\mathbf{r}_i, \mathbf{r}_k) \ln p(\mathbf{r}_i, \mathbf{r}_k) d\mathbf{r}_i d\mathbf{r}_k + k_b \int p(\mathbf{r}_j, \mathbf{r}_k) \ln p(\mathbf{r}_j, \mathbf{r}_k) d\mathbf{r}_j d\mathbf{r}_k d\mathbf{r}_j \\ &- k_B \int p(\mathbf{r}_i) \ln p(\mathbf{r}_i) d\mathbf{r}_i - k_B \int p(\mathbf{r}_j) \ln p(\mathbf{r}_j) d\mathbf{r}_j - k_B \int p(\mathbf{r}_k) \ln p(\mathbf{r}_k) d\mathbf{r}_k \end{aligned} \tag{22}$$

.[26–28]

Accordingly, one may write successive approximations of the configurational entropy as, e.g.,

$$\begin{aligned} S_c^{(1)} &= \sum_{i=1}^{N} S_{c,i}^{(1)} \\ S_c^{(2)} &= S_c^{(1)} - \sum_{i=1}^{N} \sum_{j>i}^{N} I_{ij} \\ S_c^{(3)} &= S_c^{(2)} + \sum_{i=1}^{N} \sum_{j>i}^{N} \sum_{k>j}^{N} I_{ijk} \end{aligned} \tag{23}$$

The configurational entropy associated with atom i, S_i, then follows from the same logic used above to associate a potential energy with a given atom; i.e., S_i is the 1-body entropy of atom i plus half of atom i's 2-body terms with all other atoms, plus a third of its 3-body terms, etc.:

$$\begin{aligned} S_c &= \sum_{i=1}^{N} S_{c,i} \\ S_{c,i} &= S_{c,i}^{(1)} - I_i^{(2)} + I_i^{(3)} + \ldots \\ I_i^{(2)} &= \frac{1}{2} \sum_{j \neq i}^{N} I_{ij} \\ I_i^{(3)} &= \frac{1}{3} \sum_{j \neq i}^{N} \sum_{\substack{k \neq i \\ k>j}}^{N} I_{ijk} \end{aligned} \tag{24}$$

Here $I_i^{(m)}$ denotes the sum of all mth order mutual information terms involving atom i, and we note that individual mutual information terms are not changed by permuting their indices; e.g., $I_{ijk} = I_{ikj}$. The alternation of signs of successive mutual information contributions merely reflects the sign convention used in defining these terms. Finally, we obtain a decomposition of the full entropy by combining Equations 17 and 24:

$$\begin{aligned} S &= \sum_{i=1}^{N} S_i \\ S_i &= S_{c,i} + S_{nc,i} \end{aligned} \tag{25}$$

Note that $S_{nc,i}$ is perhaps best regarded as a contribution to the one-body entropy, because it is unaffected by statistical dependencies among atoms, so

$$S_i^{(1)} = S_{c,i}^{(1)} + S_{nc,i}^{(1)} \tag{26}$$

As done in prior work on entropy expansions,[34,36] we now check whether this formulation gives the correct entropy for an ideal gas of indistinguishable atoms in the absence of an external field. In this case, all mutual information terms are identically zero, because

the atomic PDFs are statistically independent so, for example, $p(\mathbf{r}_i, \mathbf{r}_j) = p(\mathbf{r}_i)p(\mathbf{r}_j)$, and we are left with the following expression for the entropy of the ideal gas:

$$S_{ig} = S_{nc} - Nk_B \int p(\mathbf{r}_i) \ln p(\mathbf{r}_i) d\mathbf{r}_i \tag{27}$$

Due to the absence of an external field, $p(\mathbf{r}_i) = \frac{1}{V}$, and the fact that all atoms are indistinguishable means that $\Lambda_i = \Lambda_j = \Lambda$ for all i, j, and that $N_{perm} = N!$, so

$$S_{ig} = Nk_B \left(\frac{3}{2} + \ln \frac{V}{\Lambda^3} \right) - k_B \ln N! \tag{28}$$

which is the correct result for finite N. Finally, taking the limit of large N via Stirling's approximation, which says that $\lim_{N\to\infty} \ln N! = N \ln N - N$, we obtain:

$$\begin{aligned} \lim_{N\to\infty} S_{ig} &= Nk_B \left(\frac{3}{2} + \ln \frac{V}{\Lambda^3} \right) - (Nk_B \ln N - Nk_B) \\ &= Nk_B \left(\frac{5}{2} + \ln \frac{V}{N\Lambda^3} \right) \end{aligned} \tag{29}$$

which is, as hoped, the Sackur-Tetrode equation.

2.4.2 Spatial Mapping of the Entropy Density

Just as we were interested in a spatial mapping of the potential energy density (Section 2.3.2), so we are interested in a spatial mapping of the entropy density. We construct this as the sum of a configurational entropy density and a nonconfigurational entropy density:

$$S(\mathbf{R}) = S_c(\mathbf{R}) + S_{nc}(\mathbf{R}) \tag{30}$$

where

$$\begin{aligned} S_{nc}(\mathbf{R}) &= \sum_{i=1}^{N} S_{nc,i}(\mathbf{R}) \\ S_{nc,i}(\mathbf{R}) &= \int \delta(\mathbf{R} - \mathbf{r}_i) p(\mathbf{r}_i) S_{nc,i} \, d\mathbf{r}_i \end{aligned} \tag{31}$$

and $S_{nc,i}$ is given by Equation 18.

The configurational entropy density as a function of position, $S_c(\mathbf{R})$, is constructed as

follows for terms to second order:

$$
\begin{aligned}
S_c(\mathbf{R}) &= \sum_{i=1}^{N} S_{c,i}(\mathbf{R}) \\
S_{c,i}(\mathbf{R}) &= S_{c,i}^{(1)}(\mathbf{R}) - I_i^{(2)}(\mathbf{R}) + \ldots \\
S_{c,i}^{(1)}(\mathbf{R}) &= -k_B \int \delta(\mathbf{R}-\mathbf{r}_i) p(\mathbf{r}_i) \ln p(\mathbf{r}_i) d\mathbf{r}_i \\
I_i^{(2)}(\mathbf{R}) &= \frac{1}{2} \sum_{j \neq i}^{N} I_{\bar{i}j}(\mathbf{R}) \\
I_{\bar{i}j}(\mathbf{R}) &= -k_B \int \delta(\mathbf{R}-\mathbf{r}_i) p(\mathbf{r}_i,\mathbf{r}_j) \ln \frac{p(\mathbf{r}_i)p(\mathbf{r}_j)}{p(\mathbf{r}_i,\mathbf{r}_j)} d\mathbf{r}_i d\mathbf{r}_j \\
&= -k_B \int \delta(\mathbf{R}-\mathbf{r}_i) p(\mathbf{r}_i,\mathbf{r}_j) \Big[\ln p(\mathbf{r}_i) + \ln p(\mathbf{r}_j) - \ln p(\mathbf{r}_i,\mathbf{r}_j) \Big] d\mathbf{r}_i d\mathbf{r}_j \\
&= -k_B \int \delta(\mathbf{R}-\mathbf{r}_i) p(\mathbf{r}_i) \ln p(\mathbf{r}_i) d\mathbf{r}_i \\
&\quad - k_B \int \delta(\mathbf{R}-\mathbf{r}_i) p(\mathbf{r}_i,\mathbf{r}_j) \ln p(\mathbf{r}_j) d\mathbf{r}_i d\mathbf{r}_j \\
&\quad + k_B \int \delta(\mathbf{R}-\mathbf{r}_i) p(\mathbf{r}_i,\mathbf{r}_j) \ln p(\mathbf{r}_i,\mathbf{r}_j) d\mathbf{r}_i d\mathbf{r}_j
\end{aligned}
\tag{32}
$$

Here, the overline on i in $I_{\bar{i}j}(\mathbf{R})$ indicates that this is the atom where the ij mutual information is considered to be localized; we have, again, used delta functions to pick out the contribution of atom i at location $\mathbf{R}$ as detailed in Section 2.2; and we have made use of the fact that

$$
\int p(r,r') \ln p(r) dr' = \ln p(r) \int p(r,r') dr' = p(r) \ln p(r) \tag{33}
$$

The second term in the final expression may be interpreted by writing

$$
\delta(\mathbf{R}-\mathbf{r}_i) p(\mathbf{r}_i,\mathbf{r}_j) \ln p(\mathbf{r}_j) = \delta(\mathbf{R}-\mathbf{r}_i) p(\mathbf{r}_i|\mathbf{r}_j) p(\mathbf{r}_j) \ln p(\mathbf{r}_j) \tag{34}
$$

Thus, we are integrating the entropy contribution of atom j at $\mathbf{r}_j$, weighted by the probability of finding atom i at $\mathbf{r}_i$ given that j is at $\mathbf{r}_j$.

The integral of $I_{\bar{i}j}(\mathbf{R})$ over space gives the total mutual information between atoms i and j; i.e.,

$$
\int I_{\bar{i}j}(\mathbf{R}) \, d\mathbf{R} = I_{ij} \tag{35}
$$

because, for any function $f(\mathbf{r})$,

$$
\int \left[\int \delta(\mathbf{R}-\mathbf{r}) f(\mathbf{r}) d\mathbf{r} \right] d\mathbf{R} = \int f(\mathbf{r}) d\mathbf{r} \tag{36}
$$

The factor of $\frac{1}{2}$ in Equation 32 prevents double-counting of the ij mutual information densities associated with atoms i and j.

2.5 Mapping the Helmholtz and Gibbs Free Energies

We can now write the Helmholtz free energy, A as the sum of the Helmholtz free energies of atoms i,

$$\begin{aligned} A &= \sum_{i=1}^{N} A_i \\ A_i &= U_i - TS_i \end{aligned} \tag{37}$$

or as the integral of the Helmholtz free energy density as a function of position,

$$\begin{aligned} A &= \int A(\mathbf{R}) d\mathbf{R} \\ A(\mathbf{R}) &= U(\mathbf{R}) - TS(\mathbf{R}) \end{aligned} \tag{38}$$

The Gibbs free energy differs from the Helmholtz free energy by addition of PV, the product of the system pressure and volume. This quantity may be mapped to individual atoms by using the virial expression for the pressure:[37,38]

$$PV = Nk_BT + \frac{1}{3}\langle \mathcal{W}(\mathbf{r}^N) \rangle \tag{39}$$

where:

$$\begin{aligned} \mathcal{W}(\mathbf{r}^N) &= \frac{1}{2}\sum_{i=1}^{N}\sum_{j\neq i}^{N} \mathbf{r}_{ij} \cdot \mathbf{f}_{ij}(\mathbf{r}^N) \\ \langle \mathcal{W}(\mathbf{r}^N) \rangle &= \int \mathcal{W}(\mathbf{r}^N) p(\mathbf{r}^N) d\mathbf{r}^N \end{aligned} \tag{40}$$

where $\mathbf{r}_{ij}$ is the vector from atom j to atom i, and $\mathbf{f}_{ij}(\mathbf{r}^N)$ is the central force on atom i due to the presence of atom j, with the understanding that a potential function with 3-body or higher order terms must be re-expressed in terms of central forces in order for this expression to be applied.[39] Note that $\mathbf{r}_{ij}$ is a function of $\mathbf{r}^N$, although we have not written this explicitly.

We now decompose the virial on an atomic basis as

$$\mathcal{W}_i(\mathbf{r}^N) = \frac{1}{2}\sum_{j\neq i}^{N} \mathbf{r}_{ij} \cdot \mathbf{f}_{ij}(\mathbf{r}^N) \tag{41}$$

so that $\mathcal{W}(\mathbf{r}^N) = \sum_i^N \mathcal{W}_i(\mathbf{r}^N)$ We can now decompose PV across atoms i as

$$(PV)_i = k_BT + \frac{1}{3}\langle \mathcal{W}_i \rangle \tag{42}$$

and accordingly write the atomic decomposition of the Gibbs free energy as

$$\begin{aligned} G &= \sum_{i=1}^{N} G_i \\ G_i &= A_i + k_BT + \frac{1}{3}\langle \mathcal{W}_i \rangle \end{aligned} \tag{43}$$

The corresponding spatial decomposition is

$$G(\mathbf{R}) = A(\mathbf{R}) + \rho(\mathbf{R})k_BT + \frac{1}{3}\langle\mathcal{W}(\mathbf{R})\rangle$$
$$\langle\mathcal{W}(\mathbf{R})\rangle = \sum_{i=1}^{N}\int \delta(\mathbf{R}-\mathbf{r}_i)p(\mathbf{r}^N)\mathcal{W}_i(\mathbf{r}^N)d\mathbf{r}^N \tag{44}$$

where $\rho(\mathbf{R})$ is the number density of atoms at $\mathbf{R}$.

2.6 Mapping Energy and Entropy by Chemical Components

We have so far focused on atom-based mappings. In contrast, IST groups the atoms of each rigid solvent molecule into a single component, whose coordinates are fully defined by the location and orientation of the molecule. This approach has advantages over the atomistic treatment because it automatically accounts for strong, intramolecular correlations (due in the case of IST to the molecule's rigidity) instead of pushing the effects of these correlations into pairwise and higher order interatomic terms in the MIE, which can be difficult to evaluate. We expect there will also be value in assigning energy and entropy to other type of chemical components, such as to each of the amino acid residues that make up a protein, or to each molecule in a molecular crystal. Here, therefore, we develop thermodynamic decompositions in terms of chemical components, where in general a component may be a single atom or a collection of atoms.

We index chemical components with subscripts $a, b, c \ldots$, the number of components is N_{comp}, and the number of atoms in component a is N_a. Every atom in the system belongs to one and only one component, and a given component may have only one atom. The location of component a, $\mathbf{r}_a(\mathbf{r}^N) = (x_a, y_a, z_a)$, may be defined, for example, as the coordinates of component a's center of mass or the coordinates of a particular atom in component a. (We have taken the liberty of overloading the symbol $\mathbf{r}$, as well as other symbols below, to avoid the need for yet additional symbols) The full coordinates of component a are $(\mathbf{r}_a, \mathbf{q}_a)$, where $\mathbf{q}_a$ represents its orientational and internal coordinates. If a has N_a atoms, then $\mathbf{q}_a$ has dimensionality $3N_a - 3$.

2.6.1 Mapping Potential Energy by Chemical Components

The mean potential energy of component a may now be defined as the sum of the mean potential energies of its atoms:

$$U_a = \sum_{i\in a}^{N_a} U_i \tag{45}$$

where U_i is defined in Equation 9, and the summation is over atoms i belonging to component a. Because the components are non-overlapping, $U = \sum_{a=1}^{N_{comp}} U_a$.

The potential energy density, in terms of components, is

$$U(\mathbf{R}) = \sum_{a=1}^{N_{comp}} U_a(\mathbf{R}) \tag{46}$$

where the contribution of component a to the spatial energy density at $\mathbf{R}$ is

$$U_a(\mathbf{R}) = \int \left[\delta(\mathbf{R} - \mathbf{r}_a(\mathbf{r}^N))\, p(\mathbf{r}^N) \sum_{i \in a}^{N_a} U_i(\mathbf{r}^N) \right] d\mathbf{r}^N \tag{47}$$

2.6.2 Mapping Entropy by Chemical Components

The entropy of component a is given by the sum of its nonconfigurational and configurational components:

$$S_a = S_{nc,a} + S_{c,a} \tag{48}$$

and the entropy density in terms of components is given by the corresponding terms:

$$S(\mathbf{R}) = S_{nc}(\mathbf{R}) + S_c(\mathbf{R}) \tag{49}$$

Note that this $S(\mathbf{R})$ is, in general, different from that provided by the purely atomistic decomposition.

The nonconfigurational part of the entropy of chemical component a is written simply as:

$$S_{nc,a} = \sum_{i \in a}^{N_a} S_{nc,i} \tag{50}$$

where $S_{nc,i}$ is defined in Eq 17, and the spatial density of the nonconfigurational entropy is

$$\begin{aligned} S_{nc}(\mathbf{R}) &= \sum_{a=1}^{N_{comp}} S_{nc,a}(\mathbf{R}) \\ S_{nc,a}(\mathbf{R}) &= \int \delta(\mathbf{R} - \mathbf{r}_a) p(\mathbf{r}_a) S_{nc,a}\, d\mathbf{r}_a \end{aligned} \tag{51}$$

where $p(\mathbf{r}_a)$ is the PDF of the location of component a.

We now develop the configurational part of the entropy of chemical component a. To do this, we consider the distributions over $\mathbf{q}_a$ to be conditional on $\mathbf{r}_a$: $p(\mathbf{r}_a, \mathbf{q}_a) = p(\mathbf{q}_a|\mathbf{r}_a)p(\mathbf{r}_a)$, just as prior work considers the orientational distribution of a rigid solvent molecule to be conditional on the molecule's position.[2,33] By analogy with the atomistic entropy mappings in Sections 2.4.1 and 2.4.2, we write the first order configurational entropy contribution of component a as

$$\begin{aligned} S_{c,a}^{(1)} &= -k_B \int p(\mathbf{q}_a|\mathbf{r}_a) p(\mathbf{r}_a) \ln\big[p(\mathbf{q}_a|\mathbf{r}_a) + \ln p(\mathbf{r}_a)\big] d\mathbf{r}_a d\mathbf{q}_a \\ &= -k_B \int p(\mathbf{r}_a) \ln p(\mathbf{r}_a) d\mathbf{r}_a + \int p(\mathbf{r}_a) S_a^q(\mathbf{r}_a) d\mathbf{r}_a \\ S_a^q(\mathbf{r}_a) &= -k_B \int p(\mathbf{q}_a|\mathbf{r}_a) \ln p(\mathbf{q}_a|\mathbf{r}_a) d\mathbf{q}_a \end{aligned} \tag{52}$$

and the contribution of a to the first order entropy density at $\mathbf{R}$ is again picked out with a delta function at $\mathbf{r}_a$:

$$S_{c,a}^{(1)}(\mathbf{R}) = -k_B \int \delta(\mathbf{R}-\mathbf{r}_a) p(\mathbf{r}_a) \ln p(\mathbf{r}_a) d\mathbf{r}_a + \int \delta(\mathbf{R}-\mathbf{r}_a) p(\mathbf{r}_a) S_a^q(\mathbf{r}_a) d\mathbf{r}_a \tag{53}$$

The first term on the right is the first-order translational entropy density of component a, and the second term is the probability-weighted orientational+internal entropy of a as a function of location.

Summing over components then gives the total first order estimate of the configurational entropy density:

$$S_c^{(1)}(\mathbf{R}) = \sum_{a=1}^{N_{comp}} S_{c,a}^{(1)}(\mathbf{R}) \tag{54}$$

The second-order estimate of the configurational entropy of component a is

$$S_{c,a}^{(2)} = S_{c,a}^{(1)} - \frac{1}{2} \sum_{b \neq a}^{N_{comp}} I_{ab} \tag{55}$$

where I_{ab}, the mutual information between components a and b, may be written as

$$\begin{aligned} I_{ab} &= S_{c,a}^{(1)} + S_{c,b}^{(1)} + k_B \int p(\mathbf{r}_a, \mathbf{q}_a, \mathbf{r}_b, \mathbf{q}_b) \ln p(\mathbf{r}_a, \mathbf{q}_a, \mathbf{r}_b, \mathbf{q}_b) d\mathbf{r}_a d\mathbf{r}_b d\mathbf{q}_a d\mathbf{q}_b \\ &= S_{c,a}^{(1)} + S_{c,b}^{(1)} + k_B \int p(\mathbf{q}_a, \mathbf{q}_b | \mathbf{r}_a, \mathbf{r}_b) p(\mathbf{r}_a, \mathbf{r}_b) \big[\ln p(\mathbf{q}_a, \mathbf{q}_b | \mathbf{r}_a, \mathbf{r}_b) + \ln p(\mathbf{r}_a, \mathbf{r}_b) \big] d\mathbf{r}_a d\mathbf{r}_b d\mathbf{q}_a d\mathbf{q}_b \\ &= S_{c,a}^{(1)} + S_{c,b}^{(1)} + k_B \int p(\mathbf{r}_a, \mathbf{r}_b) \ln p(\mathbf{r}_a, \mathbf{r}_b) d\mathbf{r}_a d\mathbf{r}_b - \int p(\mathbf{r}_a, \mathbf{r}_b) S_{ab}^q(\mathbf{r}_a, \mathbf{r}_b) d\mathbf{r}_a d\mathbf{r}_b \\ S_{ab}^q(\mathbf{r}_a, \mathbf{r}_b) &= -k_B \int p(\mathbf{q}_a, \mathbf{q}_b | \mathbf{r}_a, \mathbf{r}_b) \ln p(\mathbf{q}_a, \mathbf{q}_b | \mathbf{r}_a, \mathbf{r}_b) d\mathbf{q}_a d\mathbf{q}_b \end{aligned} \tag{56}$$

Here $S_{ab}^q(\mathbf{r}_a, \mathbf{r}_b)$ is the joint entropy of the internal and orientational coordinates, $\mathbf{q}_a$ and $\mathbf{q}_b$, of components a and b conditioned on these components being located at $\mathbf{r}_a$ and $\mathbf{r}_b$.

To write the second order component-based entropy density, we need an expression for the component-based pairwise mutual information density. This involves three terms: a standard one-body entropy density for component a; a "cross-entropy" term that maps the first order entropy of component b to the location of a; and a joint entropy term, also mapped to the location of a. Thus,

$$\begin{aligned} S_c^{(2)}(\mathbf{R}) &= S_c^{(1)}(\mathbf{R}) - \sum_{a=1}^{N_{comp}} I_a^{(2)}(\mathbf{R}) \\ I_a^{(2)}(\mathbf{R}) &= \frac{1}{2} \sum_{b \neq a}^{N_{comp}} I_{\bar{a}b}(\mathbf{R}) \end{aligned} \tag{57}$$

where $I_{\bar{a}b}(\mathbf{R})$ is the mutual information density for component a located at $\mathbf{R}$:

$$\begin{aligned}
I_{\bar{a}b}(\mathbf{R}) &= -k_B \int \delta(\mathbf{R}-\mathbf{r}_a) p(\mathbf{r}_a,\mathbf{q}_a,\mathbf{r}_b,\mathbf{q}_b) \Big[\ln p(\mathbf{r}_a,\mathbf{q}_a) + \ln p(\mathbf{r}_b,\mathbf{q}_b) \\
&\quad - \ln p(\mathbf{r}_a,\mathbf{q}_a,\mathbf{r}_b,\mathbf{q}_b) \Big] d\mathbf{r}_a d\mathbf{r}_b d\mathbf{q}_a d\mathbf{q}_b \\
&= S^{(1)}_{c,a}(\mathbf{R}) \\
&\quad - k_B \int \delta(\mathbf{R}-\mathbf{r}_a) p(\mathbf{r}_a,\mathbf{q}_a,\mathbf{r}_b,\mathbf{q}_b) \ln p(\mathbf{r}_b,\mathbf{q}_b) d\mathbf{r}_a d\mathbf{r}_b d\mathbf{q}_a d\mathbf{q}_b \\
&\quad + k_B \int \delta(\mathbf{R}-\mathbf{r}_a) p(\mathbf{r}_a,\mathbf{q}_a,\mathbf{r}_b,\mathbf{q}_b) \ln p(\mathbf{r}_a,\mathbf{q}_a,\mathbf{r}_b,\mathbf{q}_b) d\mathbf{r}_a d\mathbf{r}_b d\mathbf{q}_a d\mathbf{q}_b \\
&= S^{(1)}_{c,a}(\mathbf{R}) + T_2(\mathbf{R}) - T_3(\mathbf{R})
\end{aligned} \tag{58}$$

We thus have three terms, one of which, $S^{(1)}_{c,a}(\mathbf{R})$, has already been developed and two others which may be developed as follows. We have, first:

$$\begin{aligned}
T_2(\mathbf{R}) &= -k_B \int \delta(\mathbf{R}-\mathbf{r}_a) p(\mathbf{r}_a,\mathbf{q}_a,\mathbf{r}_b,\mathbf{q}_b) \ln p(\mathbf{r}_b,\mathbf{q}_b) d\mathbf{r}_a d\mathbf{r}_b d\mathbf{q}_a d\mathbf{q}_b \\
&= -k_B \int \delta(\mathbf{R}-\mathbf{r}_a) p(\mathbf{q}_a,\mathbf{q}_b|\mathbf{r}_a,\mathbf{r}_b) p(\mathbf{r}_a,\mathbf{r}_b) \left[\ln p(\mathbf{r}_b) + \ln p(\mathbf{q}_b|\mathbf{r}_b) \right] d\mathbf{r}_a d\mathbf{r}_b d\mathbf{q}_a d\mathbf{q}_b \\
&= -k_B \int \delta(\mathbf{R}-\mathbf{r}_a) p(\mathbf{q}_a,\mathbf{q}_b|\mathbf{r}_a,\mathbf{r}_b) p(\mathbf{r}_a,\mathbf{r}_b) \ln p(\mathbf{r}_b) d\mathbf{r}_a d\mathbf{r}_b d\mathbf{q}_a d\mathbf{q}_b \\
&\quad - k_B \int \delta(\mathbf{R}-\mathbf{r}_a) p(\mathbf{q}_a,\mathbf{q}_b|\mathbf{r}_a,\mathbf{r}_b) p(\mathbf{r}_a,\mathbf{r}_b) \ln p(\mathbf{q}_b|\mathbf{r}_b) d\mathbf{r}_a d\mathbf{r}_b d\mathbf{q}_a d\mathbf{q}_b \\
&= -k_B \int \delta(\mathbf{R}-\mathbf{r}_a) p(\mathbf{r}_a,\mathbf{r}_b) \ln p(\mathbf{r}_b) d\mathbf{r}_a d\mathbf{r}_b + \int \delta(\mathbf{R}-\mathbf{r}_a) p(\mathbf{r}_a,\mathbf{r}_b) S^{cross}_{ab}(\mathbf{r}_a,\mathbf{r}_b) d\mathbf{r}_a d\mathbf{r}_b \\
S^{cross}_{ab}(\mathbf{r}_a,\mathbf{r}_b) &= -k_B \int p(\mathbf{q}_b|\mathbf{r}_a,\mathbf{r}_b) \ln p(\mathbf{q}_b|\mathbf{r}_b) d\mathbf{q}_b
\end{aligned} \tag{59}$$

Here, $S^{cross}_{ab}(\mathbf{r}_a,\mathbf{r}_b)$ is the internal and orientational entropy of component b when components a and b are at $\mathbf{r}_a$ and $\mathbf{r}_b$, respectively, and we have used the fact that

$$\int \delta(\mathbf{R}-\mathbf{r}_a) p(\mathbf{q}_a,\mathbf{q}_b|\mathbf{r}_a,\mathbf{r}_b) \ln p(\mathbf{q}_b|\mathbf{r}_b) d\mathbf{q}_a = \delta(\mathbf{R}-\mathbf{r}_a) p(\mathbf{q}_b|\mathbf{r}_a,\mathbf{r}_b) \ln p(\mathbf{q}_b|\mathbf{r}_b) \tag{60}$$

For the third term, we write:

$$\begin{aligned}
T_3(\mathbf{R}) &= -k_B \int \delta(\mathbf{R}-\mathbf{r}_a) p(\mathbf{r}_a,\mathbf{q}_a,\mathbf{r}_b,\mathbf{q}_b) \ln p(\mathbf{r}_a,\mathbf{q}_a,\mathbf{r}_b,\mathbf{q}_b) d\mathbf{r}_a d\mathbf{r}_b d\mathbf{q}_a d\mathbf{q}_b \\
&= -k_B \int \delta(\mathbf{R}-\mathbf{r}_a) p(\mathbf{q}_a,\mathbf{q}_b|\mathbf{r}_a,\mathbf{r}_b) p(\mathbf{r}_a,\mathbf{r}_b) \left[\ln p(\mathbf{r}_a,\mathbf{r}_b) + \ln p(\mathbf{q}_a,\mathbf{q}_b|\mathbf{r}_a,\mathbf{r}_b) \right] d\mathbf{r}_a d\mathbf{r}_b d\mathbf{q}_a d\mathbf{q}_b \\
&= -k_B \int \delta(\mathbf{R}-\mathbf{r}_a) p(\mathbf{r}_a,\mathbf{r}_b) \ln p(\mathbf{r}_a,\mathbf{r}_b) d\mathbf{r}_a d\mathbf{r}_b + \int \delta(\mathbf{R}-\mathbf{r}_a) p(\mathbf{r}_a,\mathbf{r}_b) S^{q}_{ab}(\mathbf{r}_a,\mathbf{r}_b) d\mathbf{r}_a d\mathbf{r}_b \\
S^{q}_{ab}(\mathbf{r}_a,\mathbf{r}_b) &= -k_B \int p(\mathbf{q}_a,\mathbf{q}_b|\mathbf{r}_a,\mathbf{r}_b) \ln p(\mathbf{q}_a,\mathbf{q}_b|\mathbf{r}_a,\mathbf{r}_b) d\mathbf{q}_a d\mathbf{q}_b
\end{aligned} \tag{61}$$

Here, $S^q_{ab}(\mathbf{r}_a, \mathbf{r}_b)$ is the joint internal and orientational entropy of components a and b when components a and b are at $\mathbf{r}_a$ and $\mathbf{r}_b$, respectively.

The total mutual information density associated with component a at $\mathbf{R}$ thus may be written as

$$\begin{aligned} I_{\bar{a}b}(\mathbf{R}) = &-k_B \int \delta(\mathbf{R}-\mathbf{r}_a) p(\mathbf{r}_a) \ln p(\mathbf{r}_a) d\mathbf{r}_a + \int \delta(\mathbf{R}-\mathbf{r}_a) p(\mathbf{r}_a) S^q_a(\mathbf{r}_a) d\mathbf{r}_a \\ &- k_B \int \delta(\mathbf{R}-\mathbf{r}_a) p(\mathbf{r}_a,\mathbf{r}_b) \ln p(\mathbf{r}_b) d\mathbf{r}_a d\mathbf{r}_b + \int \delta(\mathbf{R}-\mathbf{r}_a) p(\mathbf{r}_a,\mathbf{r}_b) S^{cross}_{ab}(\mathbf{r}_a,\mathbf{r}_b) d\mathbf{r}_a d\mathbf{r}_b \\ &- k_B \int \delta(\mathbf{R}-\mathbf{r}_a) p(\mathbf{r}_a,\mathbf{r}_b) \ln p(\mathbf{r}_a,\mathbf{r}_b) d\mathbf{r}_a d\mathbf{r}_b + \int \delta(\mathbf{R}-\mathbf{r}_a) p(\mathbf{r}_a,\mathbf{r}_b) S^q_{ab}(\mathbf{r}_a,\mathbf{r}_b) d\mathbf{r}_a d\mathbf{r}_b \end{aligned} \tag{62}$$

Comparison with the corresponding atomistic mutual information density shows that the first term in each line of Equation 62 has the same form as a corresponding line at the end of Equation 32, with $\mathbf{r}_a$ and $\mathbf{r}_b$ substituted for i, and j, respectively. These three terms define the translational mutual information density associated with component a, while the second term in each line of Equation 62 is a probability-weighted contribution from the internal+orientational coordinates of components a and b.

Just as for the atomistic entropy density in Eq 32, and for the same mathematical reason, the spatial integral of this mutual information density recovers the total mutual information between components a and b; i.e.,

$$\int I_{\bar{a}b}(\mathbf{R})\, d\mathbf{R} = I_{ab} \tag{63}$$

The present approach to defining the mutual information aligns with the treatment in IST (Section 3), but it is rather complex. The Supporting Information provides a simpler alternative formulation that may be of interest.

3 Relationship of GTM theory to IST

IST and its theoretical antecedents have been enormously productive, providing practical computational tools for drug design and contributing to the conceptual foundation on which the present work builds. It is thus of particular interest to analyze how GTM theory relates to IST. Because IST was derived for the special case of a solvent composed of N identical molecules interacting with a pair potential, we compare GTM theory with IST in this simplified, yet still informative, setting, and we further simplify by making the solvent monatomic and by considering entropy terms to only second order. The first appearance of an expression for the IST free energy density seems to be Eq 41 of a 2003 paper by Lazaridis and Karplus;[32] this was obtained by simply omitting the integrations over $\mathbf{r}'$ from the corresponding equations for solvation energy and entropy (see their Eqs 35-38). An apparently equivalent formulation can also be inferred from a 2006 paper;[40] see local integrals in their Equations 9 and 10 and the sum in their Equation 20.

3.1 Relationship to Energy Density in IST

For the case of interest, our first order instantaneous energy term, $u_i(\mathbf{r}_i)$, corresponds to IST's $u_{sw}(\mathbf{r})$, while our $u_{ij}(\mathbf{r}_i, \mathbf{r}_j)$ corresponds to IST's $u_{ww}(\mathbf{r}, \mathbf{r}')$. Here, as prefigured in Section 2.2, we adopt the notation of IST by moving away from the use of delta functions to map from atomic positions to coordinates of the density fields and instead allow $\mathbf{r}$ to represent both an atomic position in a PDF and the argument of a potential energy or entropy density, while $\mathbf{r}'$ is the position of a second atom in a PDF. Thus,

$$\begin{aligned} U(\mathbf{r}) &= NU_i(\mathbf{r}) \\ U_i(\mathbf{r}) &= p(\mathbf{r})u_{sw}(\mathbf{r}) + \frac{1}{2}(N-1)\int p(\mathbf{r}, \mathbf{r}')u_{ww}(\mathbf{r}, \mathbf{r}')d\mathbf{r}' \\ U(\mathbf{r}) &= \rho(\mathbf{r})u_{sw}(\mathbf{r}) + \frac{1}{2}\int \rho(\mathbf{r}, \mathbf{r}')u_{ww}(\mathbf{r}, \mathbf{r}')d\mathbf{r}' \end{aligned} \tag{64}$$

where i is the index of any solvent atom, all being equivalent, $\rho(\mathbf{r})$ is the number density of solvent at $\mathbf{r}$, $\rho(\mathbf{r}, \mathbf{r}')$ is the density of solvent pairs across locations $\mathbf{r}$ and $\mathbf{r}'$, and we have used the facts that $\rho(\mathbf{r}) = Np(\mathbf{r})$ and $\rho(\mathbf{r}, \mathbf{r}') = N(N-1)p(\mathbf{r}, \mathbf{r}')$. The corresponding IST expression from Lazaridis and Karplus is:

$$U(\mathbf{r}) = \rho g(\mathbf{r})u_{sw}(\mathbf{r}) + \frac{1}{2}\rho^2 g(\mathbf{r})\int g(\mathbf{r}')g(\mathbf{r}, \mathbf{r}')u_{ww}(\mathbf{r}, \mathbf{r}')d\mathbf{r}' \tag{65}$$

where we have omitted the subtraction of the pure solvent energy, because we are interested in the mean potential energy, rather than the solvation energy. Here, as stated immediately below their Eq 38, $\rho = \frac{N}{V}$ is the solvent number density, $\rho g(\mathbf{r}) = \rho(\mathbf{r})$, and $g(\mathbf{r}, \mathbf{r}') = \frac{\rho(\mathbf{r}, \mathbf{r}')}{\rho(\mathbf{r})\rho(\mathbf{r}')}$. It is readily verified that this IST expression is identical to the GTM theory one in Equation 64.

3.2 Relationship to Entropy Density in IST

We now compare the entropy density expressions provided by GTM theory with those of IST. In order to elucidate the relationship between the treatments of entropy in GTM theory and IST, we consider not only the entropy density for a general monatomic fluid (Section 3.2.2) but also the total entropy in the ideal gas limit (Section 3.2.3), where the atomic distributions become statistically independent of each other.

Some expectations for the outcome of this comparison may be set by noting that GTM theory is composed of entropy density contributions having the general form $S(r) = -k_B\rho(r)\ln p(r)$, where $\rho(r)$ is the number density, and $p(r)$ is a PDF and hence is normalized to 1, as expected for the standard Gibbs-Shannon entropy;[35] whereas IST expresses the entropy in an analogous series expansion, but its terms have the general form $S'(r) = -k_B\rho(r)\ln g(r)$, where $g(r)$ is proportional to $p(r)$ but is not normalized to unity. As a consequence, the IST expressions generate extraneous terms: if the constant of proportionality is a, we have $g(r) = ap(r)$, so $S'(r) = S(r) - k_B\rho(r)\ln a$. For example, as detailed below, the first order IST entropy density is $-k_B\rho(\mathbf{r})\ln g(\mathbf{r}) = -k_B\rho(\mathbf{r})[\ln p(\mathbf{r}) - \ln V]$, rather than $-k_B\rho(\mathbf{r})\ln p(\mathbf{r})$. These extra $\ln a$ terms lead to complications not encountered in GTM theory.

3.2.1 Second Order GTM Entropy Density for Monatomic Solvent

We start with the GTM theory configurational entropy density (Section 2.4), rewritten, for the sake of comparison with IST, by using $\mathbf{r}$ both for the location of an atom and for the location where the density is to be determined, and using $\mathbf{r}'$ for the position of a second, indistinguishable, atom. We also dispense with the delta function formulation, again in keeping with the notation of IST, and use the facts that all Λ_i are the same and so may be substituted by Λ; and that all N atoms are indistinguishable so the summations over atoms may be replaced by simple factors of N. Making the second order approximation, we have:

$$\begin{aligned}
S(\mathbf{r}) &\approx S_c^{(2)}(\mathbf{r}) + S_{nc}(\mathbf{r}) \\
S_c^{(2)}(\mathbf{r}) &= S_c^{(1)}(\mathbf{r}) - I^{(2)}(\mathbf{r}) \\
S_c^{(1)}(\mathbf{r}) &= -k_B N p(\mathbf{r}) \ln p(\mathbf{r}) \\
I^{(2)}(\mathbf{r}) &= -\frac{k_B\, N(N-1)}{2} \int p(\mathbf{r},\mathbf{r}') \big[\ln p(\mathbf{r}) + \ln p(\mathbf{r}') - \ln p(\mathbf{r},\mathbf{r}')\big] d\mathbf{r}' \\
S_{nc}(\mathbf{r}) &= N k_B \left[\frac{3}{2} - \ln \Lambda^3 - \frac{\ln N!}{N}\right] p(\mathbf{r})
\end{aligned} \tag{66}$$

We have used the facts that all $\Lambda_i = \Lambda$ are the same, $N_{perm} = N!$, and $p(\mathbf{r}) = \frac{1}{V}$, but we have not taken the limit of large N.

3.2.2 Second Order IST Entropy Density for a Monatomic Solvent

The original papers leading to and defining IST[2,34,36] provide the *total* entropy of the system but not the entropy *density*; it is the last three lines of Eq 41 of Lazaridis and Karplus 2003[32] that appear to be the most explicit original definition of the second order solvation entropy density in IST. This particular expression also is helpfully simplified because it omits any orientational or conformational entropy contributions, so the entropic contribution to the free energy is interpretable as the solvation entropy density of a monatomic fluid around a rigid solute. In using this expression, we do not subtract the pure solvent entropy because we are interested in the absolute entropy, not the solvation entropy. Note, too, that the entropy densities provided for IST omit the non-configurational entropy contribution, but IST expressions for total entropy[2,3] do include this contribution, as further detailed in the subsections below.

Making the required adjustments and re-rendering the equation in terms that better

match our notation, we obtain:

$$
\begin{aligned}
S^{(1)}_{IST}(\mathbf{r}) &= -k_B\rho g(\mathbf{r}) \ln g(\mathbf{r}) \\
S^{(2)}_{IST}(\mathbf{r}) &= S^{(1)}_{IST}(\mathbf{r}) - I^{(2)}_{IST}(\mathbf{r})
\end{aligned}
$$

$$
\begin{aligned}
I^{(2)}_{IST}(\mathbf{r}) &= \frac{1}{2}k_B\rho^2 g(\mathbf{r}) \int g(\mathbf{r}') \left[g(\mathbf{r},\mathbf{r}') \ln g(\mathbf{r},\mathbf{r}') - g(\mathbf{r},\mathbf{r}') + 1 \right] d\mathbf{r}' \\
&= I^{(2)}_{IST,1}(\mathbf{r}) + I^{(2)}_{IST,2}(\mathbf{r})
\end{aligned}
$$

$$
\begin{aligned}
I^{(2)}_{IST,1}(\mathbf{r}) &= \frac{1}{2}k_B\rho^2 g(\mathbf{r}) \int g(\mathbf{r}') g(\mathbf{r},\mathbf{r}') \ln g(\mathbf{r},\mathbf{r}') d\mathbf{r}' \\
I^{(2)}_{IST,2}(\mathbf{r}) &= -\frac{1}{2}k_B\rho^2 g(\mathbf{r}) \int g(\mathbf{r}') \left[g(\mathbf{r},\mathbf{r}') - 1 \right] d\mathbf{r}'
\end{aligned} \tag{67}
$$

We have broken $I^{(2)}_{IST}(\mathbf{r})$ into two parts, $I^{(2)}_{IST,1}(\mathbf{r})$ and $I^{(2)}_{IST,2}(\mathbf{r})$, for separate analysis. Note, too, that the IST expressions for entropy density omit the non-configurational entropy, S_{nc}, as further discussed below. We now rewrite these expressions in term of PDFs, to enable direct comparison with the corresponding expressions from GTM theory, above, by using the identities provided immediately following Equation 65, above. The first order term gives

$$
S^{(1)}_{IST}(\mathbf{r}) = -k_B N p(\mathbf{r}) \ln p(\mathbf{r}) - k_B N p(\mathbf{r}) \ln V \tag{68}
$$

The second term here corresponds to the $\ln a$ term mentioned in the second paragraph of Section 3.2.

We consider the two parts of the second order term separately: The first integral in the second order term gives:

$$
\begin{aligned}
I^{(2)}_{IST,1}(\mathbf{r}) &= \frac{1}{2}k_B\rho(\mathbf{r}) \int \rho(\mathbf{r}') \frac{\rho(\mathbf{r},\mathbf{r}')}{\rho(\mathbf{r})\rho(\mathbf{r}')} \ln \frac{\rho(\mathbf{r},\mathbf{r}')}{\rho(\mathbf{r})\rho(\mathbf{r}')} d\mathbf{r}' \\
&= \frac{1}{2}k_B \int \rho(\mathbf{r},\mathbf{r}') \ln \frac{\rho(\mathbf{r},\mathbf{r}')}{\rho(\mathbf{r})\rho(\mathbf{r}')} d\mathbf{r}' \\
&= \frac{k_B N(N-1)}{2} \int p(\mathbf{r},\mathbf{r}') \ln \frac{(N-1)p(\mathbf{r},\mathbf{r}')}{Np(\mathbf{r})p(\mathbf{r}')} d\mathbf{r}' \\
&= \frac{k_B N(N-1)}{2} \int p(\mathbf{r},\mathbf{r}') \left[\ln p(\mathbf{r},\mathbf{r}') - \ln p(\mathbf{r}) - \ln p(\mathbf{r}') + \ln \frac{N-1}{N} \right] d\mathbf{r}' \\
&= \frac{k_B N(N-1)}{2} \int p(\mathbf{r},\mathbf{r}') \left[\ln p(\mathbf{r},\mathbf{r}') - \ln p(\mathbf{r}) - \ln p(\mathbf{r}') \right] d\mathbf{r}' \\
&+ \frac{k_B N(N-1)}{2} p(\mathbf{r}) \ln \frac{N-1}{N}
\end{aligned} \tag{69}
$$

Thus, we have an initial term identical to $I^{(2)}(\mathbf{r})$ from GTM theory (see Equation 65) and an additional term resulting in part from the fact that $\rho(\mathbf{r},\mathbf{r}')$ is not normalized.

The second integral in the second order term gives:

$$\begin{aligned} I^{(2)}_{IST,2}(\mathbf{r}) &= -\frac{k_B}{2}\int \left[\rho(\mathbf{r},\mathbf{r}') - \rho(\mathbf{r})\rho(\mathbf{r}')\right] d\mathbf{r}' \\ &= -\frac{k_B}{2}\left[N(N-1)p(\mathbf{r}) - N^2 p(\mathbf{r})\right] \\ &= \frac{Nk_B}{2}p(\mathbf{r}) \end{aligned} \tag{70}$$

Assembling the results gives the second order term in IST,

$$\begin{aligned} I^{(2)}_{IST}(\mathbf{r}) &= I^{(2)}_{IST,1}(\mathbf{r}) + I^{(2)}_{IST,2}(\mathbf{r}) \\ &= \frac{k_B N(N-1)}{2}\int p(\mathbf{r},\mathbf{r}')\left[\ln p(\mathbf{r},\mathbf{r}') - \ln p(\mathbf{r}) - \ln p(\mathbf{r}')\right] d\mathbf{r}' \\ &+ \frac{k_B N(N-1)}{2}p(\mathbf{r})\ln\frac{N-1}{N} + \frac{Nk_B}{2}p(\mathbf{r}) \end{aligned} \tag{71}$$

and the IST estimate of the entropy density to second order is:

$$\begin{aligned} S^{(2)}_{IST}(\mathbf{r}) &= S^{(1)}_{IST}(\mathbf{r}) - I^{(2)}_{IST,1}(\mathbf{r}) - I^{(2)}_{IST,2}(\mathbf{r}) \\ &= -k_B N p(\mathbf{r})\ln p(\mathbf{r}) - k_B N p(\mathbf{r})\ln V \\ &- \frac{k_B N(N-1)}{2}\int p(\mathbf{r},\mathbf{r}')\left[\ln p(\mathbf{r},\mathbf{r}') - \ln p(\mathbf{r}) - \ln p(\mathbf{r}')\right] d\mathbf{r}' \\ &- \frac{k_B N p(\mathbf{r})}{2}\left[(N-1)\ln\frac{N-1}{N} + 1\right] \end{aligned} \tag{72}$$

We are now in a position to compare the full second-order entropy estimate from GTM theory, $S^{(2)}(\mathbf{r})$ in Eq 66, with the corresponding IST quantity, $S^{(2)}_{IST}(\mathbf{r})$ in Eq 72:

$$S^{(2)}_{IST}(\mathbf{r}) = S^{(2)}(\mathbf{r}) + D_1(\mathbf{r}) + D_2(\mathbf{r})$$

$$\begin{aligned} D_1(\mathbf{r}) &= -k_B\rho(\mathbf{r})\ln V - S_{nc}(\mathbf{r}) \\ D_2(\mathbf{r}) &= -\frac{k_B N p(\mathbf{r})}{2}\left[(N-1)\ln\frac{N-1}{N} + 1\right] \end{aligned} \tag{73}$$

where we have kept the extra first-order term, $D_1(\mathbf{r})$, separate from the extra second order term, $D_2(\mathbf{r})$. For convenience, Table 2 provides direct comparisons of the first- and second-order entropy densities provided by GTM theory, and by IST in terms of correlation functions and of PDFs. If we set aside $S_{nc}(\mathbf{r})$, which seems to have been deliberately excluded from the IST density, we are left with a difference between first-order IST and GTM theory of $D'_1(\mathbf{r}) = -k_B\rho(\mathbf{r})\ln V$. As noted above, the deviations of IST from GTM theory, $D'_1(\mathbf{r})$ and $D_2(\mathbf{r})$, derive in part from the $\ln a$ terms mentioned in the second paragraph of Section 3.2.

The additional IST terms do not have an obvious physical interpretation, and as we show below, they prevent the second- and higher-order terms from vanishing for an ideal gas, despite the absence of particle-particle correlations in this setting. By contrast, entropy terms above first order vanish identically for GTM theory, as they should. Differences between IST and GTM theory are explored further in Section 3.2.3.

Theory	Order	Entropy density term
GTM theory	1	$-k_B N p(\mathbf{r}) \ln p(\mathbf{r}) + N k_B \left[\frac{3}{2} - \ln \Lambda^3 - \frac{\ln N!}{N}\right] p(\mathbf{r})$
IST (g)	1	$-k_B \rho g(\mathbf{r}) \ln g(\mathbf{r})$
IST (p)	1	$-k_B N p(\mathbf{r}) \ln p(\mathbf{r}) - k_B N p(\mathbf{r}) \ln V$
GTM theory	2	$\frac{k_B N(N-1)}{2} \int p(\mathbf{r},\mathbf{r}') \left[\ln p(\mathbf{r},\mathbf{r}') - \ln p(\mathbf{r}) - \ln p(\mathbf{r}')\right]$
IST (g)	2	$\frac{1}{2} k_B \rho^2 g(\mathbf{r}) \int g(\mathbf{r}') \left[g(\mathbf{r},\mathbf{r}') \ln g(\mathbf{r},\mathbf{r}') - g(\mathbf{r},\mathbf{r}') + 1\right] d\mathbf{r}'$
IST (p)	2	$\frac{k_B N(N-1)}{2} \int p(\mathbf{r},\mathbf{r}') \left[\ln p(\mathbf{r},\mathbf{r}') - \ln p(\mathbf{r}) - \ln p(\mathbf{r}')\right] d\mathbf{r}'$ $+ \frac{k_B N p(\mathbf{r})}{2} \left[(N-1) \ln \frac{N-1}{N} + 1\right]$

Table 2: Comparison of the first order contribution (Order 1) and the second order contribution (Order 2) to the pairwise estimate of the entropy density in GTM theory, in IST expressed in terms of correlation functions g, and in IST expressed in terms of PDFs p. Note that the first order GTM expression includes the non-configurational entropy density, $N k_B \left[\frac{3}{2} - \ln \Lambda^3 - \frac{\ln N!}{N}\right] p(\mathbf{r})$, whereas IST includes a non-configurational component only in its expressions for the total entropy of the system, not in its density expressions.

3.2.3 Comparing GTM theory with IST for an Ideal Gas

Here we further characterize the differences between IST and GTM theory for the case of an ideal gas of identical atoms, as done before in a similar setting.[36] Because there is no solute, and hence no solute reference frame, the coordinates here are referenced to a lab frame.

For GTM theory at second order, using Eq 66 and the facts that, for the ideal gas, $p(\mathbf{r}) = \frac{1}{V}$ and $p(\mathbf{r},\mathbf{r}') = p(\mathbf{r})p(\mathbf{r}')$, due to the statistical independence of the atomic motions, and we obtain the following entropy density:

$$S^{(2)}(\mathbf{r}) = S^{(1)}(\mathbf{r}) = \frac{3k_B\rho}{2} + k_B\rho \ln \frac{V}{\Lambda^3} - \frac{k_B}{V} \ln N! \tag{74}$$

Integrating over volume to get the system entropy gives

$$S^{(2)} = \frac{3}{2} N k_B + N k_B \ln \frac{V}{\Lambda^3} - k_B \ln N! \tag{75}$$

which is the correct expression for finite N. Taking the limit of large N by using Stirling's approximation, $\ln N! \to N \ln N - N$, gives the standard Sackur-Tetrode equation:

$$S^{(2)} = N k_B \left[\frac{5}{2} - \ln(\rho \Lambda^3)\right] \tag{76}$$

Thus, the GTM entropy density gives the exact ideal gas entropy for both finite and infinite N, consistent with our conclusion for the structural decomposition of entropy in Section 2.4.1. Because mutual information terms above second order also go to zero for the case of the ideal gas, GTM theory gives the correct ideal gas entropy for all orders of the MIE.

For IST at second order, two steps are required to obtain the total entropy of an ideal gas. First, we evaluate and integrate $S^{(2)}_{IST}(\mathbf{r})$ over volume, as done for the GTM expression. Using Equation 72 with $p(\mathbf{r}) = \frac{1}{V}$ and $p(\mathbf{r}, \mathbf{r}') = p(\mathbf{r})p(\mathbf{r}')$, we obtain:

$$\begin{aligned} S^{(1)}_{IST}(\mathbf{r}) &= 0 \\ S^{(2)}_{IST}(\mathbf{r}) &= D_2(\mathbf{r}) \\ S^{(2)}_{IST} &= \int S^{(2)}_{IST}(\mathbf{r}) d\mathbf{r} = -\frac{k_B N}{2}\left[(N-1)\ln\frac{N-1}{N} + 1\right] \end{aligned} \tag{77}$$

Second, we add in the non-configurational entropy term provided in IST expressions for the total entropy,[2,3] i.e., $Nk_B\left[\frac{5}{2} - \ln(\rho\Lambda^3)\right]$, which is recognizable as, precisely, the ideal gas entropy provided by the Sackur-Tetrode equation. Thus, the total ideal gas entropy provided by IST is

$$S^{(2)}_{IST} = Nk_B\left[\frac{5}{2} - \ln(\rho\Lambda^3)\right] - \frac{k_B N}{2}\left[(N-1)\ln\frac{N-1}{N} + 1\right] \tag{78}$$

This expression appears to be incorrect not only for finite N, but also in the thermodynamic limit of infinite N, where it is straightforward to show that the second term goes not to zero, but to $-\frac{k_B}{4}$.

4 Mapping the Binding Thermodynamics of Tyrosine Kinase 2 with Congeneric Ligands

We illustrate the potential application of GTM theory to ligand binding and drug design by mapping atomistic thermodynamic contributions to the binding of Tyrosine Kinase 2 (TYK2) with the highest- and lowest-affinity inhibitors from the Protein-Ligand Benchmark Dataset by Hahn et al.[41] As shown in Figure 3, compounds jmc23 and ejm43 bind TYK2 with K_i values of 2.5 nM[42] and 840 nM,[43] respectively. Prior simulation-based relative binding free energy calculations have been shown to replicate this difference in affinity.[44] The two ligands are identical except for the moieties shown at the far left, which is a fluorocyclopropyl group in jmc23 and an isopropyl group in ejm43.

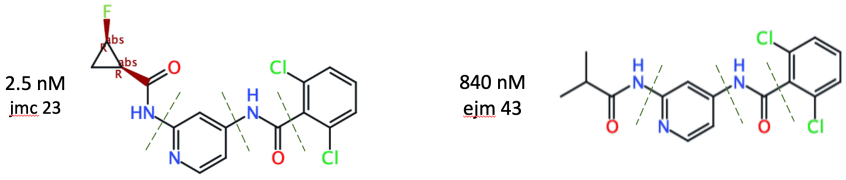

Figure 3: Tyk2 ligands analyzed in case study. Dashed green lines indicate the division of the compounds used in the strain analysis (Section 4.2.2).

4.1 Computational Methods

The following two subsections describe how the thermodynamic mappings were generated and visualized. Further methodological details are provided in Supporting Information and in a separate publication.[45]

4.1.1 Thermodynamic Mapping Analysis

The saved trajectories were used to carry out GTM calculations. Average atomic energies, U_i, of the protein and ligands were computed via the purpose-implemented `enedecomp` command of the MD analysis program `cpptraj`.[46,47] First order atomic configurational entropies, $S^{(1)}_{c,i}$, were estimated by applying the nearest-neighbor (NN) method[48–50] to the torsion angles in a complete bond-angle-torsion coordinate system.[28] The `enedecomp` tool and the NN implementation are detailed elsewhere.[45] This illustrative study includes solute-water interaction energies but omits water-water interaction energies, water entropy, and the entropy associated with relative motions of the bound protein and ligand. These contributions will be addressed in future works.

4.1.2 Visualization

A potential application of GTM theory is to show where the main contributions to binding affinity arise, identifying the regions of the protein and ligand that are energetically or entropically strained or relieved on binding. Such maps could guide ligand design by indicating which moieties anchor the ligand and should be retained, which impose a free energy penalty and are candidates for modification, and which parts of the binding site remain thermodynamically passive and might be exploited to gain new interactions.

We visualized both atomistic and spatial mappings to gain insight into contributions to the binding of the two Tyk 2 ligands. Atoms were colored according to their thermodynamic contributions. Because we found that atomic contributions can vary sharply from one atom to the next, we smoothed them prior to visualization either by summing the contributions of chemical groups of interest, or by using a graph diffusion method that allows the contributions of individual atoms to spread along the molecular graph (Supporting Information). We generated spatial distributions by mapping unsmoothed GTM atomic contributions to the simulation starting structure of each TYK2-ligand complex, and using a Gaussian kernel method (Supporting Information) to generate three-dimensional gridded densities in Data Explorer files suitable for visualization.

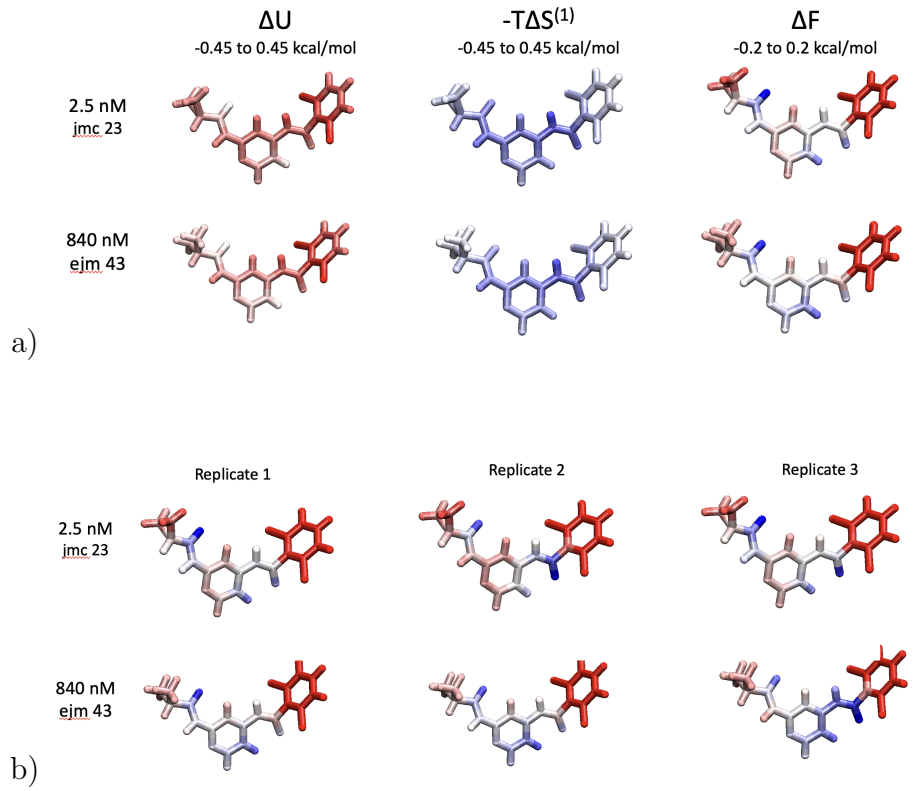

Figure 4: Contributions of ligand atoms to changes in thermodynamic quantities on binding to TYK2. Reds indicate negative changes (favoring binding) and blues indicate positive changes (opposing binding). a) Changes in mean potential energy, entropy, and free energy, as labeled, for atoms of jmc23 (top row) and ejm43 (bottom row). Limits of the color spectra are indicated in each column. GTM calculations use replicate 1 of each respective protein-ligand complex for the bound state, and these results for the complexes are referenced to the averages over all three replicates of each respective free ligand and over all six replicates of the free protein. b) Examination of convergence of the free energy mapping. Each column depicts the atomic free energy contributions computed from a different replicate calculation of the ligand-protein complex, each referenced again to averages over the appropriate free ligand and free protein simulations. The Replicate 1 results in panel (b) are the same as the free energy results in panel (a).

4.2 Results

4.2.1 Mapping the Changes in Energy, Entropy, and Free Energy on Binding

We first examine the contributions of ligand atoms to binding by subtracting the mean atomic energies, entropies, and free energies, of the free ligands and protein from those of the bound complexes for each ligand, jmc23 and mj43. As shown in Figure 4a, the energy changes of the ligand atoms uniformly favor binding, the entropy changes uniformly oppose binding, and the free energy changes afford a more complex picture. In particular, the strong red color of the chlorinated phenyl groups suggests that these are important anchors for the ligands in the binding site. The middle part of each ligand does not appear to make a decisive contribution, given its near-white color.

Perhaps most interesting is that the redder hue of fluoropropyl group in jmc23 than the isopropyl group in ejm43 indicates a stronger contribution to binding, consistent with the experimental (and computational[44]) observation that jmc23 is the tighter binder. This result is consistent across all three replicate calculations of the respective complexes, as shown in Figure 4b.

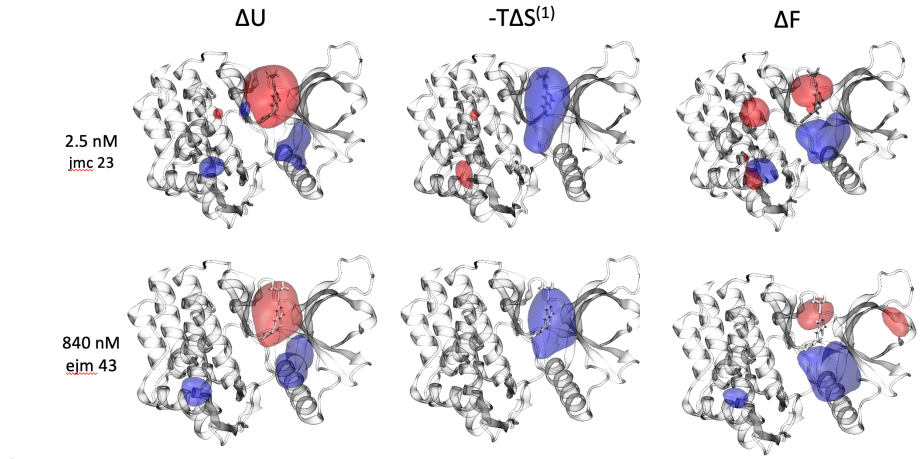

a.

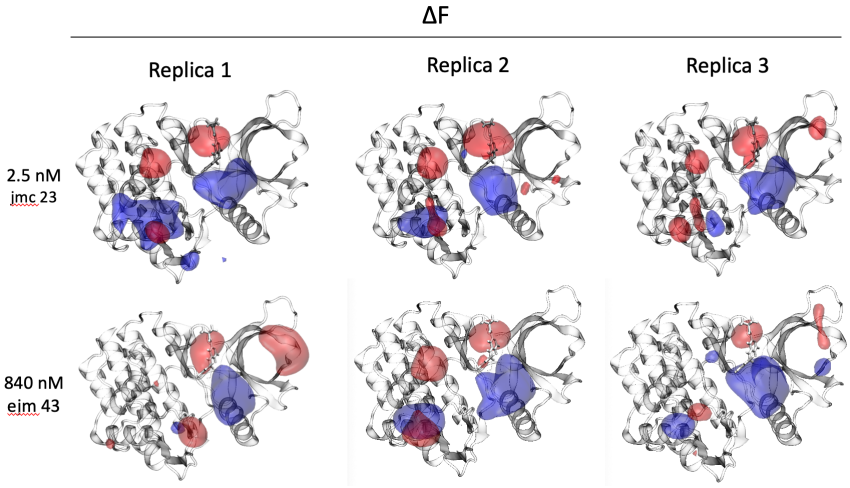

b.

Figure 5: Spatial densities of thermodynamic binding contributions. Red contours: -0.003 kcal/mol/$\AA^3$. Blue contours: 0.003 kcal/mol/$\AA^3$. a. Densities of the changes on binding in potential energy, entropy, and free energy as labeled, for ligands jmc23 (top row) and ejm43 (bottom row). Results shown are averages over all pertinent replicates. b. Free energy densities computed with the three replicates of each bound complex, referenced to averaged results for the free ligands (three replicates) and free protein (six replicates).

Next, we examine the distribution of atomic contributions to binding thermodynamics across the architectures of the two protein-ligand complexes. As shown in Figure 5a, binding of either ligand sets up a pattern of thermodynamic "strain energy" across the proteins, with both unfavorable and favorable regions. The patterns are quite similar

across both ligands. The energy density favors binding (red contours) in the region of the ligand and binding site, but disfavors binding in a region below and right of the binding site as well as in an isolated location below and left. The entropy changes in the region of the ligand and binding site disfavor binding, and — much as in Figure 4 — the pattern is more complicated for the free energy density, with favorable contributions in the immediate area of the ligand, along with a clear and consistent region opposing binding below and to the right of the binding site. This appears to be a region of the structure where going from the apo to the complexed conformation of the protein generates a free energy penalty that results from both a rise in potential energy and a drop in entropy. It is also of interest that the high affinity ligand (top row) has an additional region of favorable free energy to the left of the binding site. Examination of the potential energy and entropy densities shows that both are favorable at this location, which apparently contributes to the greater affinity of jmc23 versus ejm43, despite its distance from the binding site. It is also interesting that the largely α-helical top left region of the protein makes little contribution – favorable or unfavorable—to binding for either ligand, and thus may be thought of as structurally important but relatively passive from a thermodynamic standpoint.

As shown in Figure 5b, the overall patterns just discussed are largely consistent across replicates of the bound complexes for each ligand. However, there are relatively wide variations across replicates at the lower left of the structure and in a loop region to the right of the binding site. These are regions where, for reasons yet to be determined, larger fluctuations lead to slower convergence of these GTM maps.

4.2.2 Mapping Ligand and Protein Valence Strain

The use of a force field with separate energy contributions (e.g., valence *versus* non-bonded terms) allows us to further decompose atomic energies by type. We illustrate this by mapping the changes in valence strain energy – here defined as the sum of bond-stretch, angle-bend, and dihedral terms – of the ligand and protein binding site upon binding each of the two ligands, jmc23 and ejm43. As shown in Figure 6, the flexible portions of both ligands are under reduced internal strain when the ligands are bound than when they are free in solution. The change is more marked for the higher-affinity ligand, jmc23, with the difference focused, not surprisingly, in the moieties that differ between the two compounds. Little difference is visible in the nearby binding site residues. We used conformational clustering of the unbound ligands in water to look for any preferred conformations with notable valence strain, but found none (data not shown). Instead, it appears that the bound ligands are held in low-strain conformations, while thermal fluctuations in solution allow the ligands to sample a range of conformations with moderately elevated valence strain.

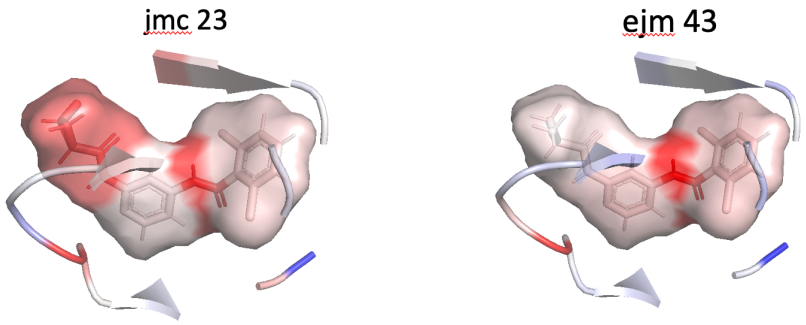

Figure 6: Changes on binding of the valence energy (bond-stretch, bond-angle, and dihedral force field terms) of the high- and low-affinity ligands jmc23 and ejm43 respectively, and of the protein binding site, color coded onto atoms and molecular surfaces. Ligand results are summed by chemical fragment (see green dashed lines in Figure 3) and protein results are summed by residue. Ligand strain values are highly reproducible across the three independent replicate simulations (jmc23 total: -2.32 +/- 0.06 kcal/mol; ejm43 total: -1.61 +/- 0.08 kcal/mol). Binding site protein strain shows larger inter-replicate variability (std 1.6 kcal/mol) but the difference between the two ligands remains highly significant (Z = 6.1). Darkest red corresponds to -0.250 kcal/mol/atom, darkest blue corresponds to +0.250 kcal/mol/atom.

5 Discussion

We have described the first broadly applicable structural and spatial decompositions of the potential energy, entropy, and free energy, derived from fundamental classical statistical thermodynamics. The resulting expressions satisfy desiderata mentioned in the Introduction and previously,[25] namely that the spatial integral of the free energy density over the entire system should give the correct system free energy, that the free energy density should go to zero where the spatial number density of atoms goes to zero, and that all entropy terms above first order should go to zero in the absence of correlation. Our application of the MIE in an integrated fashion across both the solute and the solvent unites our prior work applying the MIE to liquids,[25] where it essentially took the place of IST's entropy expansion, and to proteins,[28] where we used it to study changes in configurational entropy on protein-peptide binding.[24] Because of this integration, GTM theory is applicable to not only the solvent but also the solute in a solute-solvent system.

We furthermore illustrated the application of GTM theory to protein-ligand binding with a case study centered on binding of two compounds to the known drug target TYK2. We found that GTM indicates which parts of a ligand and protein favor or oppose binding or, alternatively, that represent relatively passive bystanders. It also shows promise toward explaining affinity differences in terms of structural elements and force field energy terms. GTM theory should also be applicable to other types of systems, including solids and lipid membranes. In addition, by proving the feasibility of writing well-grounded expressions for local thermodynamic quantities, and by connecting them clearly with widely understood principles of probability theory, as opposed to

the more specialized correlation functions used in liquid state theory, the present work opens opportunities for further work that may lead to improved formulations of these quantities.

In the past, the solvent-only theory IST has been used to gain insight into the role of water in protein-ligand binding and thus guide ligand design, via analysis of molecular simulations with tools such as WaterMap,[51] GIST[33,52] SSTMap,[53] and STOW.[54] We anticipate that the present generalized theory will provide further insight into the contributions of various parts of the protein and ligand to their binding free energy and thus enable new tools for structure-based drug design. It may also provide a new window into other phenomena, such as how point-mutations affect protein stability, the thermodynamics of grain boundaries and defects in solids, and how energy flows in allosteric proteins and molecular motors. In particular, as noted in the Introduction, allostery and other binding-induced molecular motions may be associated with a localized rise in free energy around the binding site, followed by a structural relaxation that mediates function.

Given the central role that IST and related theory have played in developing this field, it is useful to define the relationship between GTM theory and IST. The GTM treatment of the potential energy density is similar to that of IST, but is generalized to arbitrary potential functions for flexible molecules. The GTM treatment of the entropy density writes the entropy in terms of normalized PDFs instead of non-normalized n-particle correlation functions, $g_N^{(n)}$, as done in IST. Using PDFs avoids the generation of extraneous terms which make IST inexact. For example, IST yields nonzero second- and higher-order entropy terms for an ideal gas and thus risks giving the incorrect impression that the particles correlate. In contrast, as shown in Section 3.2.3, GTM theory gives the exact ideal gas entropy. Expressing entropy in terms of PDFs also simplifies the application of GTM theory for different ensembles, makes GTM theory simpler conceptually and mathematically, enables a unified treatment of entropy density for an entire solute-solvent system, and makes the theory more accessible to researchers who are familiar with PDFs but not with correlation functions. Thus, we hope that this formulation will facilitate connections to the large body of literature on the significance and calculation of the Gibbs-Shannon entropy.[50,55–60]

The present treatment of entropy density also differs from that of IST by including the non-configurational component, S_{nc}. It is reasonable that this contribution has largely been omitted in the past,[32,33,35] because the non-configurational entropy changes only for processes that change T or N. Nonetheless, we include its contribution to both the structural and spatial entropy decompositions of GTM theory in order to demonstrate the existence of a rigorous decomposition of the total entropy that is consistent with our desiderata (above), to provide a foundation for applications of GTM theory to processes where S_{nc} does change, due to changes in T or composition, and also for use with the grand canonical partition function, which is made up of canonical partition functions with different values of N.

Our atomistic decomposition of the potential energy appears to match that used by Kalayan and coworkers, who recently presented an approach to decomposing energy and entropy for a protein-water system.[61] However, although their multiscale cell correlation entropy method appears to have the merit of rapid numerical convergence, it is not

derived from the exact configurational entropy and does not reduce to a known exact result in any well-defined limit. In contrast, the MIE-based entropy in GTM theory is an exact mathematical identity whose truncation errors are, in principle, systematically improvable.

When applying GTM theory to proteins, it will be of interest to make connections with experimental studies that provide insight into changes in local entropy, such as measurements of NMR order parameters[62–65] and multiconformer refinements of room temperature protein crystallographic data.[66] Although we would not necessarily expect quantitative agreement, given the simplifying approximations inherent in each approach, it is reasonable to expect similar qualitative pictures of changes in local protein entropy induced by ligand binding or other stimuli.

In future work, we will use GTM theory to extract structural and spatial thermodynamic mappings from molecular simulation data, exploring biophysical and pharmaceutical applications of the results. We will also work to advance the state of the art in the calculation of entropy changes. For example, in going to third order, progress may be made by pruning the number of triplets that are computed, based e.g., on the pairwise mutual information values within the triplet. However, it is essential to note that many of the most compelling applications will not require tight (e.g., $\pm$ 1 kcal/mol) numerical convergence of *global* thermodynamic properties of the system. Instead, as already demonstrated by applications such as STOW,[54] WaterMap[10,51] and GIST,[11,33,67] as well as in prior application of the MIE to protein-ligand binding,[24] semi-quantitative convergence of *local* thermodynamics at first or second order is sufficient to provide physical insight and guide chemical design.

6 Conclusions

We have presented GTM theory, which provides structural and spatial decompositions of the potential energy, entropy, and free energy of a chemical system, derived from classical statistical thermodynamics via the multibody expansion of the energy and the mutual information expansion of the entropy. The resulting mappings satisfy basic desiderata: they integrate to the correct system totals, vanish where the atomic density vanishes, and yield no spurious entropy terms in the absence of correlation. Unlike IST, which applies only to the solvent and is not exact for finite N, GTM theory applies to all components of a system — solute and solvent alike — and is formally exact. An initial application to the binding of two congeneric ligands to TYK2 shows that GTM maps computed from standard molecular dynamics simulations are reasonably well converged and chemically informative: they identify parts of the ligand and protein favor or oppose binding, and they localize the affinity difference between the two ligands to the chemical group that distinguishes them. We anticipate that GTM theory will provide a useful foundation for methods to extract mechanistic and design insight from molecular simulations, in applications ranging from drug discovery, protein engineering, and material design, to the study of allostery and molecular motors.

7 Supporting Information Description

The SI provides an alternative spatial mapping of mutual information; simulation details; the method used for graph-based smoothing of atomistic mappings; and the method used for spatial representation of atomistic thermodynamic maps.

Acknowledgments

MKG thanks the NIGMS/NIH for support via grant R01-GM158907. TK thanks the NIGMS/NIH for support via grant R35-GM144089. This work does not necessarily represent the views of the NIH. DRR made use of resources from the LoBoS cluster (NIH/NHLBI). The contributions of DRR were made as part of their official duties as an NIH federal employee, are in compliance with agency policy requirements, and are considered Works of the United States Government. However, the findings and conclusions presented in this paper are those of the authors and do not necessarily reflect the views of the NIH or the U.S. Department of Health and Human Services.

Author disclosures

MKG has an equity interest in and is a cofounder and scientific advisor of VeraChem LLC. He is also on the scientific advisory boards of Denovicon Therapeutics, In Cerebro, Cold Start Therapeutics, and Beren Therapeutics.

TK is founder and scientific advisor of Deep Waters NYC, LLC; has an equity interest in Ventus Therapeutics; has an equity interest in and is a director and scientific advisor for InCerebro Inc.; and is an author on U.S. patents 7,756,674; 7,970,580, 7,970,581.

References

[1] A. Movahedi-Rad and R. Alizadeh. Simulating Grain Boundary Energy Using Molecular Dynamics. *Journal of Modern Physics*, 05(08):627–632, 2014.

[2] Themis Lazaridis. Inhomogeneous Fluid Approach to Solvation Thermodynamics. 2. Applications to Simple Fluids. *The Journal of Physical Chemistry B*, 102(18):3542–3550, 1998.

[3] Themis Lazaridis. Innhomogeneous Fluid Approach to Solvation Thermodynamics. 1. Theory. *The Journal of Physical Chemistry B*, 102(18):3531–3541, 1998.

[4] David J. Huggins, Woody Sherman, and Bruce Tidor. Rational Approaches to Improving Selectivity in Drug Design. *Journal of Medicinal Chemistry*, 55(4):1424–1444, 2012.

[5] Balázs Zoltán Zsidó and Csaba Hetényi. Water in drug design: pitfalls and good practices. *Expert Opinion on Drug Discovery*, 20(6):745–764, 2025.

[6] Marie-Pierre Collin, Mario Lobell, Walter Hübsch, Dirk Brohm, Hartmut Schirok, Rolf Jautelat, Klemens Lustig, Ulf Bömer, Verena Vöhringer, Mélanie Héroult,

Sylvia Grünewald, and Holger Hess-Stumpp. Discovery of Rogaratinib (BAY 1163877): a pan-FGFR Inhibitor. *ChemMedChem*, pages 437–445, 2018.

[7] Pierre Matricon, R. Rama Suresh, Zhan-Guo Gao, Nicolas Panel, Kenneth A. Jacobson, and Jens Carlsson. Ligand design by targeting a binding site water. *Chemical Science*, 2021.

[8] Agnieszka A. Kaczor, Agata Zięba, and Dariusz Matosiuk. The application of WaterMap-guided structure-based virtual screening in novel drug discovery. *Expert Opinion on Drug Discovery*, 19(1):73–83, 2024.

[9] Trent E. Balius, Marcus Fischer, Reed M. Stein, Thomas B. Adler, Crystal N. Nguyen, Anthony Cruz, Michael K. Gilson, Tom Kurtzman, and Brian K. Shoichet. Testing inhomogeneous solvation theory in structure-based ligand discovery. *Proceedings of the National Academy of Sciences of the United States of America*, 114(33):E6839–E6846, 2017.

[10] Robert Abel, Tom Young, Ramy Farid, Bruce J. Berne, and Richard A. Friesner. The role of the active site solvent in the thermodynamics of factor Xa-ligand binding. *Journal of the American Chemical Society*, 130(9):2817–2831, 2008.

[11] Crystal N. Nguyen, Anthony Cruz, Michael K. Gilson, and Tom Kurtzman. Thermodynamics of Water in an Enzyme Active Site: Grid-Based Hydration Analysis of Coagulation Factor Xa. *Journal of Chemical Theory and Computation*, 10(7):2769–2780, 2014.

[12] Jeffry Setiadi, Frank Biedermann, Werner M. Nau, and Michael K. Gilson. Thermodynamics of Water Displacement from Binding Sites and its Contributions to Supramolecular and Biomolecular Affinity. *Angewandte Chemie International Edition*, 64(35):e202505713, 2025.

[13] B. L. Tembe and J. A. McCammon. Ligand-Receptor Interactions. *Comput. Chem.*, 8:281–283, 1984.

[14] P. A. Bash, U. C. Singh, R. Langridge, and P. A. Kollman. Free energy calculations by computer simulation. *Science*, 236:564–568, 1987.

[15] Zoe Cournia, Bryce Allen, and Woody Sherman. Relative Binding Free Energy Calculations in Drug Discovery: Recent Advances and Practical Considerations. *Journal of Chemical Information and Modeling*, 57(12):2911–2937, 2017.

[16] Christina E. M. Schindler, Hannah Baumann, Andreas Blum, Dietrich Böse, Hans-Peter Buchstaller, Lars Burgdorf, Daniel Cappel, Eugene Chekler, Paul Czodrowski, Dieter Dorsch, Merveille K. I. Eguida, Bruce Follows, Thomas Fuchß, Ulrich Grädler, Jakub Gunera, Theresa Johnson, Catherine Jorand Lebrun, Srinivasa Karra, Markus Klein, Tim Knehans, Lisa Koetzner, Mireille Krier, Matthias Leiendecker, Birgitta Leuthner, Liwei Li, Igor Mochalkin, Djordje Musil, Constantin Neagu, Friedrich Rippmann, Kai Schiemann, Robert Schulz, Thomas Steinbrecher, Eva-Maria Tanzer, Andrea Unzue Lopez, Ariele Viacava Follis, Ansgar Wegener, and Daniel Kuhn. Large-Scale Assessment of Binding Free Energy Calculations in Active Drug Discovery Projects. *Journal of Chemical Information and Modeling*, 60(11):5457–5474, 2020.

[17] Edward King, Erick Aitchison, Han Li, and Ray Luo. Recent Developments in Free Energy Calculations for Drug Discovery. *Frontiers in Molecular Biosciences*, 8:712085, 2021.

[18] Joe Z. Wu, Solmaz Azimi, Sheenam Khuttan, Nanjie Deng, and Emilio Gallicchio. Alchemical Transfer Approach to Absolute Binding Free Energy Estimation. *Journal of Chemical Theory and Computation*, 17(6):3309–3319, 2021.

[19] C. M. Carr and P. S. Kim. A spring-loaded mechanism for the conformational change of influenza hemagglutinin. *Cell*, 73(4):823–832, 1993.

[20] Chavela Carr, Charu Chaudhry, and Peter Kim. Influenza hemagglutinin is spring-loaded by a metastable native conformation. *Proceedings of the National Academy of Sciences of the United States of America*, 94:14306–13, 1998.

[21] He Xl, Chow Dc, M M Martick, and K C Garcia. Allosteric activation of a spring-loaded natriuretic peptide receptor dimer by hormone. *Science*, 293(5535):1657–62, 2001.

[22] Daniel A. Holdbrook, Björn M. Burmann, Roland G. Huber, Maxim V. Petoukhov, Dmitri I. Svergun, Sebastian Hiller, and Peter J. Bond. A Spring-Loaded Mechanism Governs the Clamp-like Dynamics of the Skp Chaperone. *Structure*, 25(7):1079–1088.e3, 2017.

[23] Andrew T Fenley, Hari S Muddana, and Michael K Gilson. Calculation and visualization of atomistic mechanical stresses in biomolecules. *Biophysical Journal*, 106(2):461a, 2014.

[24] Benjamin J Killian, Joslyn Yudenfreund Kravitz, Sandeep Somani, Paramita Dasgupta, Yuan-Ping Pang, and Michael K Gilson. Configurational Entropy in Protein-Peptide Binding. Computational Study of Tsg101 UEV Domain with an HIV-derived PTAP Nonapeptide. *J Mol Biol*, 389(2):315–335, 2009.

[25] Michael K Gilson and Tom Kurtzman. Free energy density of a fluid and its role in solvation and binding. *Journal of Chemical Theory and Computation*, 20(7):2871–2887, 2024.

[26] Phil Attard, Owen G Jepps, and Stjepan Marcelja. Information Content of Signals using Correlation Function Expansions of the Entropy. *PHYSICAL REVIEW E*, 56, 1997.

[27] Hiroyuki Matsuda. Physical nature of higher-order mutual information: Intrinsic correlations and frustration. *Physical Review E*, 62(3):3096, 2000.

[28] Benjamin J Killian, Joslyn Yundenfreund Kravitz, and Michael K Gilson. Extraction of configurational entropy from molecular simulations via an expansion approximation. *The Journal of chemical physics*, 127(2), 2007.

[29] Donald A. McQuarrie. *Statistical Mechanics*. Harper & Row, New York, 1973.

[30] Michael J Potter and Michael K Gilson. Coordinate systems and the calculation of molecular properties. *The Journal of Physical Chemistry A*, 106(3):563–566, 2002.

[31] J. H. Irving and John G. Kirkwood. The Statistical Mechanical Theory of Transport Processes. IV. The Equations of Hydrodynamics. *The Journal of Chemical Physics*, 18(6):817–829, 1950.

[32] Themis Lazaridis and Martin Karplus. Thermodynamics of protein folding: a microscopic view. *Biophysical Chemistry*, 100(1):367–395, 2003.

[33] Crystal N. Nguyen, Tom Kurtzman Young, and Michael K. Gilson. Grid inhomogeneous solvation theory: Hydration structure and thermodynamics of the miniature receptor cucurbit[7]uril. *The Journal of Chemical Physics*, 137(4):044101, 2012.

[34] Duane C. Wallace. On the role of density fluctuations in the entropy of a fluid. *The Journal of Chemical Physics*, 87(4):2282, 1987.

[35] R.L. Stratonovich. The entropy of systems with a random number of particles. *Soviet Physics, JETP*, 28:409–421, 1955.

[36] Andras Baranyai and Denis J. Evans. Direct entropy calculation from computer simulation of liquids. *Physical Review A*, 40(7):3817, 1989.

[37] Aidan P. Thompson, Steven J. Plimpton, and William Mattson. General formulation of pressure and stress tensor for arbitrary many-body interaction potentials under periodic boundary conditions. *The Journal of Chemical Physics*, 131(15):154107, 2009.

[38] Nikhil Chandra Admal and E. B. Tadmor. Stress and heat flux for arbitrary multibody potentials: A unified framework. *The Journal of Chemical Physics*, 134(18):184106, 2011.

[39] Nikhil Chandra Admal and E. B. Tadmor. A Unified Interpretation of Stress in Molecular Systems. *Journal of Elasticity*, 100(1):63–143, 2010.

[40] Zheng Li and Themis Lazaridis. Thermodynamic Contributions of the Ordered Water Molecule in HIV-1 Protease. *J. Am. Chem. Soc.*, 125(22):6636–6637, 2003.

[41] David Hahn, Christopher Bayly, Melissa L. Boby, Hannah Bruce Macdonald, John Chodera, Vytautas Gapsys, Antonia Mey, David Mobley, Laura Perez Benito, Christina Schindler, Gary Tresadern, and Gregory Warren. Best Practices for Constructing, Preparing, and Evaluating Protein-Ligand Binding Affinity Benchmarks [Article v1.0]. *Living Journal of Computational Molecular Science*, 4(1):1497–1497, August 2022.

[42] Jun Liang, Anne van Abbema, Mercedesz Balazs, Kathy Barrett, Leo Berezhkovsky, Wade Blair, Christine Chang, Donnie Delarosa, Jason DeVoss, Jim Driscoll, Charles Eigenbrot, Nico Ghilardi, Paul Gibbons, Jason Halladay, Adam Johnson, Pawan Bir Kohli, Yingjie Lai, Yanzhou Liu, Joseph Lyssikatos, Priscilla Mantik, Kapil Menghrajani, Jeremy Murray, Ivan Peng, Amy Sambrone, Steven Shia, Young Shin, Jan Smith, Sue Sohn, Vickie Tsui, Mark Ultsch, Lawren C. Wu, Yisong Xiao, Wenqian Yang, Judy Young, Birong Zhang, Bing-yan Zhu, and Steven Magnuson. Lead Optimization of a 4-Aminopyridine Benzamide Scaffold To Identify Potent, Selective, and Orally Bioavailable TYK2 Inhibitors. *Journal of Medicinal Chemistry*, 56(11):4521–4536, 2013.

[43] Jun Liang, Vickie Tsui, Anne Van Abbema, Liang Bao, Kathy Barrett, Maureen Beresini, Leo Berezhkovskiy, Wade S. Blair, Christine Chang, James Driscoll, Charles Eigenbrot, Nico Ghilardi, Paul Gibbons, Jason Halladay, Adam Johnson, Pawan Bir Kohli, Yingjie Lai, Marya Liimatta, Priscilla Mantik, Kapil Menghrajani, Jeremy Murray, Amy Sambrone, Yisong Xiao, Steven Shia, Young Shin, Jan Smith, Sue Sohn, Mark Stanley, Mark Ultsch, Birong Zhang, Lawren C. Wu, and Steven Magnuson. Lead identification of novel and selective TYK2 inhibitors. *European Journal of Medicinal Chemistry*, 67:175–187, 2013.

[44] Lingle Wang, Yujie Wu, Yuqing Deng, Byungchan Kim, Levi Pierce, Goran Krilov, Dmitry Lupyan, Shaughnessy Robinson, Markus K. Dahlgren, Jeremy Greenwood, Donna L. Romero, Craig Masse, Jennifer L. Knight, Thomas Steinbrecher, Thijs Beuming, Wolfgang Damm, Ed Harder, Woody Sherman, Mark Brewer, Ron Wester, Mark Murcko, Leah Frye, Ramy Farid, Teng Lin, David L. Mobley, William L. Jorgensen, Bruce J. Berne, Richard A. Friesner, and Robert Abel. Accurate and Reliable Prediction of Relative Ligand Binding Potency in Prospective Drug Discovery by Way of a Modern Free-Energy Calculation Protocol and Force Field. *Journal of the American Chemical Society*, 137(7):2695–2703, 2015.

[45] Joe Cruz, Samrat Lohar, Helmut Carter, Steven Ramsey, Daniel Roe, Michael K. Gilson, and Tom Kurtzman. Atomic decomposition and mapping of solute thermodynamics. *ChemRxiv*, 10.26434/chemrxiv.15008034/v1, 2026.

[46] Daniel R. Roe and Thomas E. Cheatham. PTRAJ and CPPTRAJ: Software for Processing and Analysis of Molecular Dynamics Trajectory Data. *Journal of Chemical Theory and Computation*, 9(7):3084–3095, 2013.

[47] Daniel R. Roe and Thomas E. Cheatham. Parallelization of CPPTRAJ enables large scale analysis of molecular dynamics trajectory data. *Journal of Computational Chemistry*, 39(25):2110–2117, 2018.

[48] H. Singh, S. Misra, V Hnizdo, A. Fedorowicz, and E. Demchuk. Nearest neighbor estimates of entropy. *American Journal of Mathematical and Management Sciences*, 23:301–321, 2003.

[49] Vladimir Hnizdo, Eva Darian, Adam Fedorowicz, Eugene Demchuk, Shengqiao Li, and Harshinder Singh. Nearest-neighbor nonparametric method for estimating the configurational entropy of complex molecules. *Journal of Computational Chemistry*, 28(3):655–668, 2007.

[50] Vladimir Hnizdo, Jun Tan, Benjamin J Killian, and Michael K Gilson. Efficient calculation of configurational entropy from molecular simulations by combining the mutual-information expansion and nearest-neighbor methods. *Journal of computational chemistry*, 29(10):1605–1614, 2008.

[51] Tom Young, Robert Abel, Byungchan Kim, Bruce J. Berne, and Richard A. Friesner. Motifs for molecular recognition exploiting hydrophobic enclosure in protein-ligand binding. *Proceedings of the National Academy of Sciences of the United States of America*, 104(3):808–813, 2007.

[52] Steven Ramsey, Crystal Nguyen, Romelia Salomon-Ferrer, Ross C Walker, Michael K Gilson, and Tom Kurtzman. Solvation thermodynamic mapping of molecular surfaces in AmberTools: GIST, 2016.

[53] Kamran Haider, Anthony Cruz, Steven Ramsey, Michael K. Gilson, and Tom Kurtzman. Solvation Structure and Thermodynamic Mapping (SSTMap): An Open-Source, Flexible Package for the Analysis of Water in Molecular Dynamics Trajectories. *Journal of Chemical Theory and Computation*, 14(1):418–425, 2018.

[54] Zheng Li and Themis Lazaridis. Computing the thermodynamic contributions of interfacial water. *Methods in Molecular Biology (Clifton, N.J.)*, 819:393–404, 2012.

[55] Josiah Willard Gibbs. *Elementary Principles in Statistical Mechanics: Developed with Especial Reference to the Rational Foundation of Thermodynamics*. Cambridge Library Collection - Mathematics. Cambridge University Press, Cambridge, 2010.

[56] C. E. Shannon. A mathematical theory of communication. *The Bell System Technical Journal*, 27(3):379–423, 1948.

[57] E. T. Jaynes. Information Theory and Statistical Mechanics. *Physical Review*, 106(4):620–630, 1957.

[58] G. P. Basharin. On a Statistical Estimate for the Entropy of a Sequence of Independent Random Variables. *Theory of Probability & Its Applications*, 4(3):333–336, 1959.

[59] Lin Yuan and H. K. Kesavan. Bayesian estimation of shannon entropy. *Communications in Statistics - Theory and Methods*, 26(1):139–148, 1997.

[60] Ilaria Pia la Torre, David A. Kelly, Hector D. Menendez, and David Clark. To BEE or not to BEE: Estimating more than Entropy with Biased Entropy Estimators. *arXiv*, arXiv.2501.11395, 2025.

[61] Jas Kalayan, Arghya Chakravorty, Jim Warwicker, and Richard H. Henchman. Total free energy analysis of fully hydrated proteins. *Proteins: Structure, Function, and Bioinformatics*, 91(1):74–90, 2023.

[62] Mikael Akke, Rafael Brueschweiler, and Arthur G. Palmer. NMR order parameters and free energy: An analytical approach and its application to cooperative calcium(2+) binding by calbindin D9k. *Journal of the American Chemical Society*, 115(21):9832–9833, October 1993.

[63] Lucas Zidek, Milos V. Novotny, and Martin J. Stone. Increased protein backbone conformational entropy upon hydrophobic ligand binding. *Nat. Struct*, 6:1118–1121, 1999.

[64] A. Joshua Wand. The dark energy of proteins comes to light: Conformational entropy and its role in protein function revealed by NMR relaxation. *Curr. Opin. Struct. Biol.*, 23(1):75–81, 2013.

[65] J. J. Prompers and R. Bruschweiler. Thermodynamic interpretation of NMR relaxation parameters in proteins in the presence of motional correlations. *Journal of Physical Chemistry B*, 104(47):11416–11424, November 2000.

[66] Stephanie A. Wankowicz and James S. Fraser. Advances in uncovering the mechanisms of macromolecular conformational entropy. *Nature Chemical Biology*, 21(5):623–634, 2025.

[67] Trent E. Balius, Marcus Fischer, Reed M. Stein, Thomas B. Adler, Crystal N. Nguyen, Anthony Cruz, Michael K. Gilson, Tom Kurtzman, and Brian K. Shoichet. Testing inhomogeneous solvation theory in structure-based ligand discovery. *Proceedings of the National Academy of Sciences of the United States of America*, 114(33):E6839–E6846, 2017.

SUPPORTING INFORMATION
A Generalized Theory for the Structural and Spatial Mapping of Energy, Entropy, and Free Energy

Michael K. Gilson[*,1], Joe Cruz[2], Kunhuan Liu[1], Samrat Lohar[2], Helmut Carter[2], Daniel R. Roe[3], Tom Kurtzman[*,2]

September 4, 2026

1. Department of Pharmaceutical Sciences, Skaggs School of Pharmacy and Pharmaceutical Sciences, University of California San Diego, La Jolla, CA 92093, USA.

2. PhD Programs in Chemistry, Biochemistry, and Biology, The Graduate Center of the City University of New York, New York, 10016, USA; Department of Chemistry, Lehman College, The City University of New York, Bronx, New York, 10468, USA.

3. Laboratory of Computational Biology, National Heart, Lung, and Blood Institute, National Institutes of Health, Bethesda, Maryland, 20892, USA

* To whom correspondence should be addressed. mgilson@ucsd.edu, simpleliquid@gmail.com

1 An alternative spatial mapping of mutual information

Given the complexity of the spatial mapping of mutual information density by chemical components presented in Section 2.6.2, it may be of interest to consider a simpler alternative definition of this density. This alternative can also be applied to the atomistic mapping developed in Section 2.4.2.

Here, we write the density of the total mutual information between components a and b as

$$I_{ab}(\mathbf{R}) = S^{(1)}_{c,a}(\mathbf{R}) + S^{(1)}_{c,b}(\mathbf{R}) - S_{c,ab}(\mathbf{R}) \tag{1}$$

where we omit the overline on a present in the original formulation, i.e., $I_{\bar{a}b}(\mathbf{R})$, because the present definition treats components a and b symmetrically. Here, the first two terms in Equation 1 take their standard form (Equation52),

$$\begin{aligned} S^{(1)}_{c,a}(\mathbf{R}) &= -k_B \int \delta(\mathbf{R}-\mathbf{r}_a)p(\mathbf{r}_a)\ln p(\mathbf{r}_a)d\mathbf{r}_a + \int \delta(\mathbf{R}-\mathbf{r}_a)p(\mathbf{r}_a)S^q_a(\mathbf{r}_a)d\mathbf{r}_a \\ S^{(1)}_{c,b}(\mathbf{R}) &= -k_B \int \delta(\mathbf{R}-\mathbf{r}_b)p(\mathbf{r}_b)\ln p(\mathbf{r}_b)d\mathbf{r}_b + \int \delta(\mathbf{R}-\mathbf{r}_b)p(\mathbf{r}_b)S^q_b(\mathbf{r}_b)d\mathbf{r}_b \end{aligned} \tag{2}$$

while the joint entropy density is constructed as

$$\begin{aligned} 2S_{c,ab}(\mathbf{R}) &= -k_B \int \Big[\delta(\mathbf{R}-\mathbf{r}_a) + \delta(\mathbf{R}-\mathbf{r}_b)\Big] p(\mathbf{r}_a,\mathbf{q}_a,\mathbf{r}_b,\mathbf{q}_b)\ln p(\mathbf{r}_a,\mathbf{q}_a,\mathbf{r}_b,\mathbf{q}_b)d\mathbf{r}_a d\mathbf{r}_b d\mathbf{q}_a d\mathbf{q}_b \\ &= -k_B \int \Big[\delta(\mathbf{R}-\mathbf{r}_a) + \delta(\mathbf{R}-\mathbf{r}_b)\Big] p(\mathbf{q}_a,\mathbf{q}_b|\mathbf{r}_a,\mathbf{r}_b)p(\mathbf{r}_a,\mathbf{r}_b)\big[\ln p(\mathbf{q}_a,\mathbf{q}_b|\mathbf{r}_a,\mathbf{r}_b) \\ &\quad + \ln p(\mathbf{r}_a,\mathbf{r}_b)\big]d\mathbf{r}_a d\mathbf{r}_b d\mathbf{q}_a d\mathbf{q}_b \\ &= -k_B \int \delta(\mathbf{R}-\mathbf{r}_a)p(\mathbf{r}_a,\mathbf{r}_b)\ln p(\mathbf{r}_a,\mathbf{r}_b)d\mathbf{r}_a d\mathbf{r}_b - k_B \int \delta(\mathbf{R}-\mathbf{r}_b)p(\mathbf{r}_a,\mathbf{r}_b)\ln p(\mathbf{r}_a,\mathbf{r}_b)d\mathbf{r}_a d\mathbf{r}_b \\ &\quad + \int \delta(\mathbf{R}-\mathbf{r}_a)p(\mathbf{r}_a,\mathbf{r}_b)S^q(\mathbf{r}_a,\mathbf{r}_b)d\mathbf{r}_a d\mathbf{r}_b + \int \delta(\mathbf{R}-\mathbf{r}_b)p(\mathbf{r}_a,\mathbf{r}_b)S^q(\mathbf{r}_a,\mathbf{r}_b)d\mathbf{r}_a d\mathbf{r}_b \end{aligned}$$

$$S^q(\mathbf{r}_a,\mathbf{r}_b) = -k_B \int p(\mathbf{q}_a,\mathbf{q}_b|\mathbf{r}_a,\mathbf{r}_b)\ln p(\mathbf{q}_a,\mathbf{q}_b|\mathbf{r}_a,\mathbf{r}_b)d\mathbf{q}_a d\mathbf{q}_b \tag{3}$$

The factor of two corrects what would otherwise be a double-count of the joint entropy.

Much as in Section 2.6.2, the integral of the mutual information density returns the correct mutual information:

$$\int I_{ab}(\mathbf{R})\, d\mathbf{R} = I_{ab} \tag{4}$$

However, whereas in Section 2.6.2,

$$I_{\bar{a}b}(\mathbf{R}) \neq I_{\bar{b}a}(\mathbf{R}) \tag{5}$$

here

$$I_{ab}(\mathbf{R}) = I_{ba}(\mathbf{R}) \tag{6}$$

Thus, the two definitions of the mutual information density may be termed "asymmetric" vs. "symmetric". The asymmetric formulation aligns with IST, while the symmetric one may be simpler to code and perhaps equally useful. The chief difference lies in where each contribution is localized in space. In the asymmetric version, every term in $I_{\overline{a}b}(\mathbf{R})$, is localized at $\mathbf{r}_a$ via $\delta(\mathbf{R} - \mathbf{r}_a)$. For example, the marginal entropy contribution of component b, in term $T_2(\mathbf{R})$, appears at the location of a, weighted by the conditional probability that a is at $\mathbf{R}$ given that b is at $\mathbf{r}_b$. In the symmetric version, by contrast, the marginal entropy contribution of b is localized at $\mathbf{r}_b$ by its own delta function.

2 Simulation details

We carried out three 500 ns simulations of the bound complex of TYK2 with each ligand, three 500 ns simulations of each of the two free ligands in water, and six 500 ns of the free protein in water, where each replicate was initiated with different random velocities and random number seeds. These simulations were carried out with the OpenMM simulation package.[1]

Initial conformations of the bound complexes were assembled from the PLBenchmark-prepared TYK2 protein structure based on the 4GIH X-ray structure and the corresponding PLBenchmark Glide-docked ligand poses.[2] No additional docking, alignment, or pose generation was performed. Each free-ligand system used the same stored SDF conformer as the corresponding bound complex, without the protein, whereas each free-protein system used the same PLBenchmark-prepared protein coordinates, without a ligand. All systems were solvated in rhombic dodecahedral boxes of TIP3P water with 1.5 nm padding and 0.15 M NaCl, with additional counterions added to achieve charge neutrality. Partial charges and other force field parameters were assigned with OpenFE's `openmm_utils` package.[3] The protein force field was ff14SB,[4] the water model was TIP3P,[5] and ligand parameters were assigned from the Open Force Field Sage (openff-2.2.1) general force field,[6] with AM1-BCC[7] partial charges.

Each system was initially energy-minimized using OpenMM's `LocalEnergyMinimizer`, with the default root-mean-square force tolerance (10 $\mathrm{kJ, mol^{-1}, nm^{-1}}$) and a maximum of 5000 iterations. Following unrestrained energy minimization, velocities were assigned directly from a Maxwell-Boltzmann distribution at 298.15 K; no gradual heating protocol was applied. Systems underwent 0.1 ns of NVT equilibration at 298.15 K, followed by velocity resampling and 5 ns of NPT equilibration at 298.15 K and 1 bar. Production simulations continued from the resulting NPT-equilibrated state. Temperature was controlled using the Langevin thermostat implemented in OpenMM's `LangevinMiddleIntegrator`, and pressure was controlled using a `MonteCarloBarostat`. Each 500 ns production simulation was performed in the NPT ensemble, with trajectory data recorded every 100 ps. Appropriate structural stability of the simulations is confirmed in Figure 1, which plots the root-mean-square deviation of the free protein and the ligand-protein complexes from their starting structures.

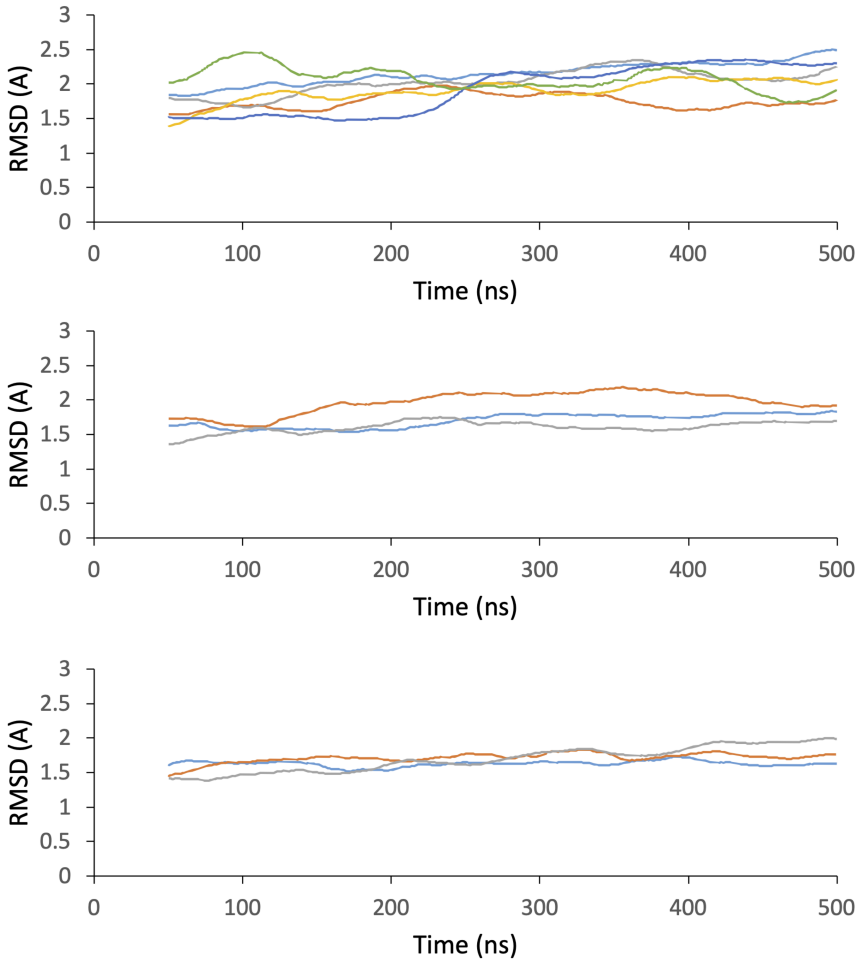

Figure 1: Structural stability of protein and complex simulations assessed via root-mean-square deviations (Å) from their respective starting configurations, following structural superposition. Results are averages over 50 ns time-windows, for snapshots saved every 100 ps. Top: six replicates of the apo protein. Middle: three replicates of the complex with jmc23. Bottom: three replicates of the complex with ejm43.

3 Graph-based smoothing of atomistic mappings

We smoothed atomic contributions across bonded neighboring atoms by allowing limited diffusive spread of the GTM terms along covalent bonds. The value x_i associated with atom i relaxes iteratively toward its bonded neighbors, where each iteration yields $x_i^{(n+1)} = x_i^{(n)} - \alpha \sum_{j \sim i}(x_i^{(n)} - x_j^{(n)})$, where n is the iteration number, $j \sim i$ indexes all atoms j covalently bonded to atom i, and α is a user-defined parameter akin to a diffusion rate. We used 10 iterations with $\alpha = 0.2$. Note that this procedure leaves $\sum_i x_i$ unchanged, and that it does not smooth across nearby atoms except if they are covalently bonded to each other.

4 Spatial representation of atomistic thermodynamic maps

We visualized atomistic mappings in terms of thermodynamic densities by the following kernel method. A Gaussian kernel was placed at each atom, where the atomic coordinates were those used to initiate the simulations of the respective complexes, and the kernel had a standard deviation 3Å and was scaled by the atomic contribution of interest. Values from these kernels were transferred to the vertices of a 3-dimensional grid with spacing 1 Å, out to a cutoff distance of three standard deviations (9Å). To ensure that the entire contribution of each atom was transferred to the grid, the grid was padded by the cutoff distance and atomic contributions were scaled to account for truncation of the Gaussians. The thermodynamic value X_i transferred from atom i to grid vertex j was scaled by $1/v$, where v is the volume of a grid box, to define a gridded spatial density g_j, so that $\sum_i X_i = v \sum_j g_j$. Note that this is not a formal implementation of the Irving-Kirkwood formalized (Section 2.2).

References

[1] Peter Eastman, Raimondas Galvelis, Raúl P. Peláez, Charlles R. A. Abreu, Stephen E. Farr, Emilio Gallicchio, Anton Gorenko, Michael M. Henry, Frank Hu, Jing Huang, Andreas Krämer, Julien Michel, Joshua A. Mitchell, Vijay S. Pande, João PGLM Rodrigues, Jaime Rodriguez-Guerra, Andrew C. Simmonett, Sukrit Singh, Jason Swails, Philip Turner, Yuanqing Wang, Ivy Zhang, John D. Chodera, Gianni De Fabritiis, and Thomas E. Markland. OpenMM 8: Molecular Dynamics Simulation with Machine Learning Potentials. *The Journal of Physical Chemistry B*, 128(1):109–116, 2024.

[2] David Hahn, Christopher Bayly, Melissa L. Boby, Hannah Bruce Macdonald, John Chodera, Vytautas Gapsys, Antonia Mey, David Mobley, Laura Perez Benito, Christina Schindler, Gary Tresadern, and Gregory Warren. Best Practices for Constructing, Preparing, and Evaluating Protein-Ligand Binding Affinity Benchmarks [Article v1.0]. *Living Journal of Computational Molecular Science*, 4(1):1497–1497, August 2022.

[3] Hannah M. Baumann, Joshua T. Horton, Michael M. Henry, Alyssa Travitz, Benjamin Ries, Richard J. Gowers, David W. H. Swenson, Iván Pulido, Dominic Rufa, David L. Dotson, Nupur Bansal, Joseph P. Bluck, Howard Broughton, Kira A. Campbell, Lili Cao, Benedikt Frieg, Vytautas Gapsys, Hendrik Göddeke, Marco Klähn, Sirish Kaushik Lakkaraju, Stephanie M. Linker, Thomas Löhr, Aniket Magarkar, Sergio Pérez-Conesa, Hans E. Purkey, Hayk Saribekyan, Jenke Scheen, Christina E. M. Schindler, Thomas Steinbrecher, Chaya D. Stern, Patricia Suriana, William C. Swope, Gary Tresadern, Lev Tsidilkovski, Binqing Wei, Alexander H. Williams, Yao Wu, Ivy Zhang, John D. Chodera, James R. B. Eastwood, David L. Mobley, and Irfan Alibay. Large-Scale Collaborative Assessment of Binding Free Energy Calculations for Drug Discovery Using OpenFE. *Journal of Chemical Information and Modeling*, 2026.

[4] James A. Maier, Carmenza Martinez, Koushik Kasavajhala, Lauren Wickstrom, Kevin E. Hauser, and Carlos Simmerling. ff14SB: Improving the Accuracy of Protein Side Chain and Backbone Parameters from ff99SB. *Journal of Chemical Theory and Computation*, 11(8):3696–3713, 2015.

[5] William L. Jorgensen, Jayaraman Chandrasekhar, Jeffry D. Madura, Roger W. Impey, and Michael L. Klein. Comparison of simple potential functions for simulating liquid water. *The Journal of Chemical Physics*, 79(2):926, 1983.

[6] Simon Boothroyd, Pavan Kumar Behara, Owen C. Madin, David F. Hahn, Hyesu Jang, Vytautas Gapsys, Jeffrey R. Wagner, Joshua T. Horton, David L. Dotson, Matthew W. Thompson, Jessica Maat, Trevor Gokey, Lee-Ping Wang, Daniel J. Cole, Michael K. Gilson, John D. Chodera, Christopher I. Bayly, Michael R. Shirts, and David L. Mobley. Development and Benchmarking of Open Force Field 2.0.0: The Sage Small Molecule Force Field. *Journal of Chemical Theory and Computation*, 2023.

[7] A Jakalian, DB Jack, and CI Bayly. Fast, efficient generation of high-quality atomic charges. AM1-BCC model: II. Parameterization and validation. *J. Comput. Chem.*, 23(16):1623–1641, 2002.